
Evaluation of Sea-ice in the Max Planck Institute Earth System Model

Michael Hübner



Munich 2013

Evaluation von Meereis im Max Planck Institute Earth System Model

Michael Hübner



München 2013

Ludwig-Maximilians-Universität München
Faculty of Physics
Meteorological Institute Munich

Evaluation of Sea-ice in the Max Planck Institute Earth System Model

Michael Hübner

BACHELOR THESIS

Supervisor: Priv.-Doz. Dr. habil. Veronika Eyring (DLR)

Deutsches Zentrum für Luft- und Raumfahrt (DLR)
Institut für Physik der Atmosphäre

March 2013

Abstract

Polar sea-ice reacts rapidly to climate changes and is therefore a good indicator for climate conditions in a warming world. To understand the Earth's climate, several climate models are being developed. In 2007 most of the models participating in the third phase of the Coupled Model Intercomparison Project (CMIP3) underestimated the decline of Arctic sea-ice extent, which is well constrained by satellite observations since the late 1970s.

The new Max Planck Institute Earth System Model (MPI-ESM), whose predecessor model also participated in CMIP3, provides several improvements regarding the simulation of sea-ice. In this thesis, sea-ice in the MPI-ESM is evaluated with observations and projections for the 21st century are analyzed for different scenarios. Simulated sea-ice is compared to the observational datasets from the Advanced Microwave Scanning Radiometer - Earth Observing System (AMSR-E) in addition to observations from the National Snow and Ice Data Center (NSIDC) and from the Hadley Centre Sea Ice and Sea Surface Temperature (HadISST).

In the Arctic region, the MPI-ESM realistically simulates the observed seasonal cycle, the spatial distribution and the summer-time trend of sea-ice extent. The model's large internal inter-annual variability is in good agreement with the observations. The MPI-ESM provides different future scenarios depending on the atmospheres greenhouse gas concentration. Under the Representative Concentration Pathways (RCP) 2.6 scenario an Arctic ice-free summer can still be avoided, while the RCP 8.5 projection simulates a strong sea-ice decrease and an ice-free summer during the second half of the 21st century.

The seasonal cycle of Antarctic sea-ice extent is realistically simulated by the MPI-ESM, but the total sea-ice amount is substantially underestimated. The relatively small simulated summer-time trend in the Southern Hemisphere sea-ice is in agreement with observations. The RCP 2.6 projection shows a decrease of March Antarctic sea-ice in the first and an increase of sea-ice in the second half of the 21st century. The simulation of RCP 8.5 projects a further decrease during the 21st century and the possibility of an ice-free Antarctic summer by the end of the century.

Overall, the MPI-ESM simulates Arctic sea-ice in agreement with observations. The causes for the biases in Antarctic sea-ice should be investigated in a future work.

Content

1.	Introduction	- 1 -
1.1.	Background and Motivation.....	- 1 -
1.2.	Structure of the Thesis.....	- 2 -
2.	Scientific Background	- 3 -
2.1.	Definition of Sea-ice and Relevance for Climate.....	- 3 -
2.2.	Representation of Sea-ice in Climate Models	- 3 -
3.	Model and Model Simulations.....	- 5 -
3.1.	Max Planck Institute Earth System Model (MPI-ESM)	- 5 -
3.1.1.	MPI-ESM Overview	- 5 -
3.1.2.	MPI-ESM Sea-ice Module	- 6 -
3.2.	Model Simulations	- 7 -
4.	Sea-ice Observations for Model Evaluation	- 9 -
4.1.	Sea-ice Observations.....	- 9 -
4.1.1.	Measurement Techniques and Retrieval	- 9 -
4.1.2.	AMSR-E	- 10 -
4.1.3.	NSIDC	- 12 -
4.1.4.	HADISST	- 12 -
4.2.	Methodology.....	- 13 -
5.	Results	- 15 -
5.1.	Arctic Sea-ice	- 15 -
5.1.1.	Evaluation of sea-ice in the Arctic.....	- 15 -
5.1.2.	September Arctic sea-ice Projections	- 19 -
5.2.	Antarctic sea-ice	- 22 -
5.2.1.	Evaluation of sea-ice in the Antarctic	- 22 -
5.2.2.	March Antarctic Sea-ice Projections.....	- 26 -
6.	Summary and Outlook	- 29 -
	Acknowledgements	- 30 -
	References	- 31 -

1. Introduction

1.1. Background and Motivation

The Intergovernmental Panel on Climate Change (IPCC) Fourth Assessment Report (AR4) concluded that warming of the climate system is unequivocal [IPCC, 2007]. During the past century, the annual mean global mean surface temperature has increased by around 0.8°C and by 0.6°C in the past three decades [Hansen *et al.*, 2006]. The concentration of carbon dioxide (CO₂) has increased dramatically in the past 50 years [Ballantyne *et al.*, 2012]. The international climate policy target is to prevent a surface temperature rise larger than 2°C with respect to the pre-industrial (1850) average value. According to the IPCC AR4, the mean Earth's temperature is projected to increase between 1.1 and 6.4°C by 2100, depending on the greenhouse gases scenario and on the exact climate sensitivity [IPCC, 2007]. Today, the first consequences of the global warming like increase in natural disasters, acidification of the oceans or glaciers melting can be observed [Wang and Chameides, 2005].

The polar regions are good indicators for changes in climate conditions. The sea-ice cover reacts rapidly to climate warming. Since 1978 the extent of sea-ice is well observed by satellites scanning these areas. The measurements show that especially the Arctic sea-ice cover decreased significantly in the past years [Stroeve *et al.*, 2007, 2012]. This reduction in observed sea-ice was faster than most of the models participating in phase three of the Coupled Model Intercomparison Project (CMIP3) predicted. In September 2012 the Arctic sea-ice extent reached the lowest value ever observed since the beginning of satellite observations [Meier, 2012].

On the other hand, the sea-ice extent in the Antarctic regions shows a smaller trend [Cavalier and Parkinson, 2008]. Several reasons for such a trend over Antarctica have been discussed in the literature (see for example Stroeve *et al.* [2007]). These include changes in wind systems which rip open spaces into the ice cover, congeal rapidly and therefore extend the net sea-ice amount [Holland and Kwok, 2012]. This process works only in the almost hermetically sealed Antarctic since in addition to increasing temperatures the geographic properties also have a significant effect. The Antarctic is a land mass totally surrounded by oceans, whereas the Arctic is a marine area, mostly enclosed by land masses. The Arctic sea-ice is therefore largely captivated and is able to form thicker, multiyear ice [Barry *et al.*, 1993]. The melting of Arctic sea-ice due to climate warming induces a positive climate feedback. While the area covered with sea-ice reflects most of the solar radiation, the exposed darker water surface absorbs the solar energy and enhances the melting. In the Southern Hemisphere, winds and oceanic streams circle around the Antarctic and lead to an isolation from the regions at lower latitudes. Recent studies have also suggested that changes in stratospheric ozone could have potential impacts on Antarctic sea-ice (Bitz and Polvani, 2012; Sigmond and Fyfe, 2010; Smith *et al.*, 2012; Turner *et al.*, 2009).

Given the importance of sea-ice in the climate system, the goal of this work is to evaluate sea-ice concentrations in the Max Planck Institute – Earth System Model (MPI-ESM) in a first

step and to provide projections of sea-ice in the 21st century for different future scenarios. This is done by a comparison to observations from multiple sources. In particular, this work focuses on including measurements from the Advanced Microwave Scanning Radiometer - Earth Observing System (AMSR-E, *Spreen et al.* [2008]) in addition to observations from the National Snow and Ice Data Center (NSIDC, *Cavalieri et al.*, [1997]) and the Hadley Centre Sea Ice and Sea Surface Temperature (HadISST, *Rayner et al.* [2003]) that have so far been frequently used in evaluation studies [e.g., *Stroeve et al.*, 2007, 2012; *Notz et al.*, 2013].

The AMSR-E data have been provided by the University of Bremen as part of the Climate Model Validation by confronting globally Essential Climate Variables from models with observations (ClimVal project, see <http://www.fona-miklip.de/en/340.php>). ClimVal is part of the BMBF MiKlip project on decadal predictions. It is a collaborative project of the DLR Institute of Atmospheric Physics and the Institute of Environmental Physics of the University of Bremen. The main goal of the ClimVal project is to quantify strengths and weaknesses as well as uncertainty of the MiKlip model system, with a focus on the representation of selected Essential Climate Variables (ECVs) that are important for decadal predictions. A satellite-based sea ice extent dataset is constructed, which is used in this work to evaluate long-term simulations with the MPI-ESM that have been performed as part of CMIP phase 5 (CMIP5) for the past and for three Representative Concentration Pathways (RCPs) in the future [*Giorgetta et al.*, 2013]. An extension of this work will be the evaluation of the decadal simulations performed with the model system.

1.2. Structure of the Thesis

Chapter 2 provides a short review of the scientific background for this work. A brief description of the MPI-ESM and its sea-Ice module is given in Chapter 3, which also describes the model simulations that are used for the evaluation and the future projections of sea-ice. The observational datasets for the evaluation of the MPI-ESM and the measurement principles as well as a description of the program code that has been developed as part of this work are described in Chapter 4. The results and conclusions of this work, separated into Arctic Sea-ice (Section 5.1) and Antarctic sea-ice (Section 5.2), are presented in Chapter 5. Chapter 6 finishes with a summary and an outlook.

2. Scientific Background

2.1. Definition of Sea-ice and Relevance for Climate

Sea-ice is a thin, fragmented layer on the polar oceans, representing the boundary between the atmosphere and the ocean and having a strong influence on their interaction. Changes in Arctic sea-ice are strongly related to cyclones, which play a central role in the interaction between the atmosphere and the Earth's surface [Murray and Simmonds, 1995].

Sea-ice changes significantly affect the marine ecosystem [Grebmeier *et al.*, 2010]. The sea-ice concentration and thickness are modified by dynamic and thermodynamic processes.

Sea-ice has a positive climate feedback [Perovich and Polashenski, 2012]. The albedo of sea-ice lies in the range between 0.65 and 0.9. After ablating, the albedo of the remaining open water is reduced to 0.05 to 0.1, thus less solar radiation is reflected and more absorbed, leading to heating of the surface. Therefore the melting of sea-ice through warming causes a further increase in surface temperature.

Due to its climate relevance the investigation and simulation of sea-ice is an important scientific topic of research. To minimize the model noise and to make the model simulations more comparable to the observational data and among each other, the sea-ice extent is used. In the sea-ice extent calculation, grid cells that have an ice concentration larger or equal to 15% are counted as completely covered.

2.2. Representation of Sea-ice in Climate Models

Figure 1 shows the Arctic September sea-ice extent simulated by models participating in CMIP3 in comparison to observations (dark red) from 1900 to 2100 (from Stroeve *et al.* [2007]). The ordinate illustrates the sea-ice extent in million square kilometers. All models exhibit a downward trend, but the observed decrease is larger than in any of the model simulations. The observed summer minima in 2006 in comparison to the mean model forecast (solid black) is approximately 30 years ahead. The figure illustrates that Arctic sea-ice decline was dramatically underestimated by the CMIP3 models. Stroeve *et al.* [2007] assumed that the effects of greenhouse gas increases and the sensitivity of the Arctic sea-ice to warming are greater than the models suggested.

The MPI-ESM predecessor model was part of the CMIP3 and also underestimated the sea-ice trend. The MPI-ESM that is analyzed in this work has been improved compared to the model used in CMIP3 (see Section 3.1.1), which is expected to lead to a better representation of the sea-ice extent.

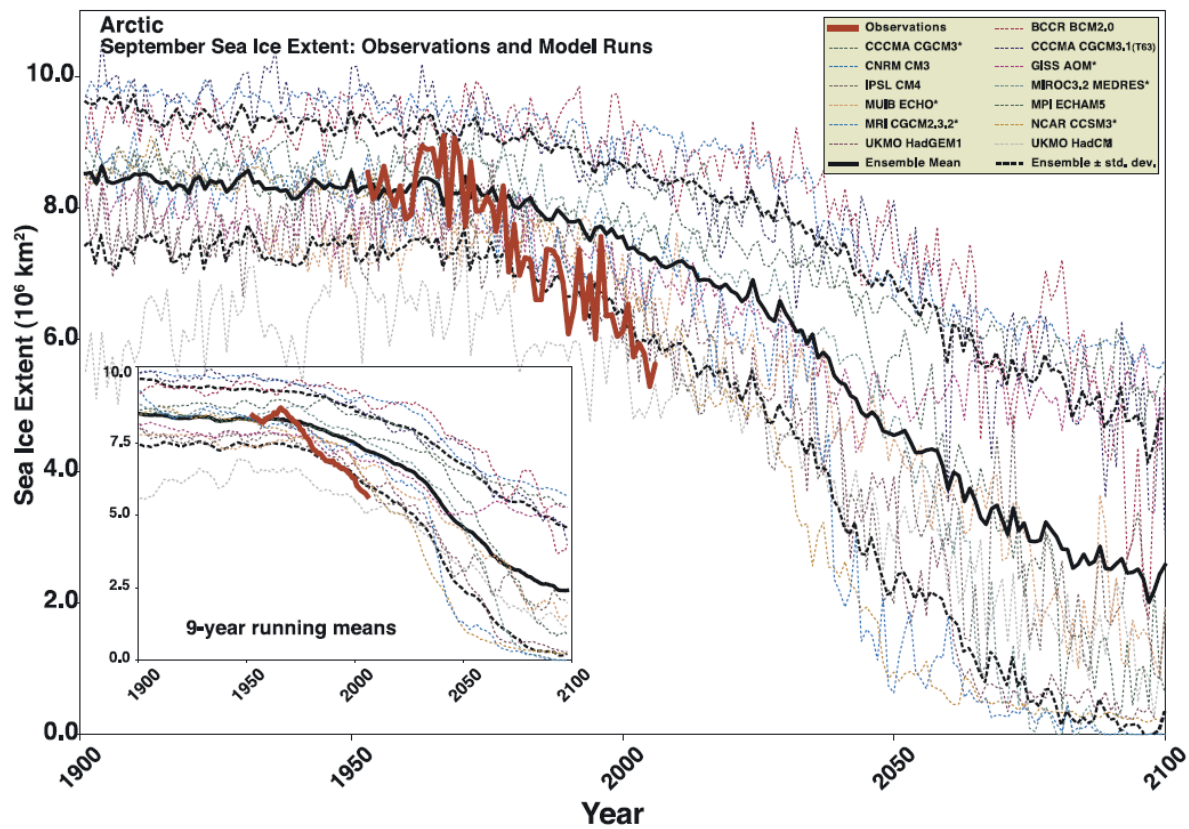


Figure 1. September Arctic Sea-ice in models participating in the CMIP3 Project. From Stroeve *et al.*, *GRL*, [2007], their Figure 1.

3. Model and Model Simulations

The model that is evaluated in this work is the Max Planck Institute Earth System Model (MPI-ESM). Section 3.1 provides a short description of the MPI-ESM. In Section 3.2, the model simulations are described.

3.1. Max Planck Institute Earth System Model (MPI-ESM)

3.1.1. MPI-ESM Overview

The Earth system model MPI-ESM consists of four parts: the coupled general circulation models for the atmosphere ECHAM6 [Stevens *et al.*, 2012] and the Max Planck Institute ocean model (MPIOM) for the ocean [Jungclaus *et al.*, 2012], the process models for land surface JSBACH [Reick *et al.*, 2012] and the HAMOCC5 [Ilyina *et al.*, 2012] ocean biogeochemistry model (see Figure 2).

The MPI-ESM is an advancement of the predecessor model ECHAM5/MPIOM [Jungclaus *et al.*, 2006] that has been used in CMIP3. The main improvement of this new version is the introduction of a coupled carbon cycle. The surface albedo, aerosol representation and the shortwave radiative transfer have also been updated. The MPI-ESM has already been used for comparative model calculations in the CMIP5 Project [Giorgetta *et al.*, 2013].

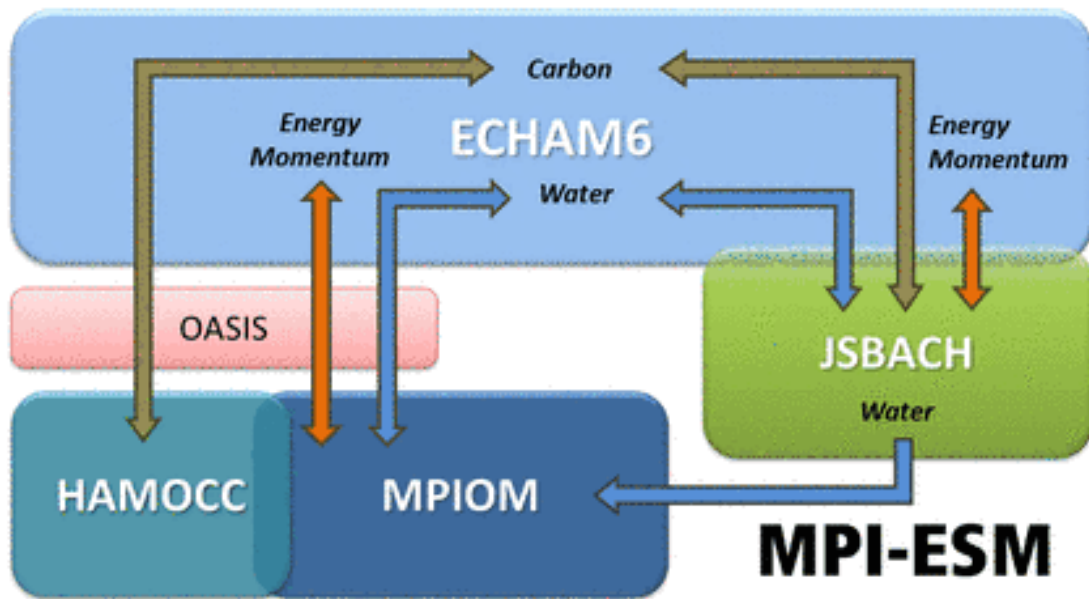


Figure 2. Sketch of the MPI-ESM modules. The blue and green boxes represent the models for oceanic (MPIOM), atmospheric (ECHAM6), ocean biogeochemistry (HAMOCC5) and land surface (JSBACH) processes. The pink box represents the coupling interface OASIS3 for exchange of momentum, energy (orange arrows), water (blue arrows) and trace gases (brown arrows).

Since the MPI-ESM was developed to answer a wide range of scientific questions regarding climate change, it is available at different resolutions. Simulations with the MPI-EMS-LR (low resolution) and MPI-ESM-MR (mixed-resolution) model configurations were used in this work. For the ocean, the MPI-ESM-LR configuration uses a 1.5° horizontal resolution, 40 vertical levels and a bipolar grid for the ocean. The poles of the LR grid are vertically mirrored and placed over Greenland in the Northern Hemisphere and over the Weddell Sea in the Southern Hemisphere. The MR configuration affords a higher resolution of 0.4° horizontal in the ocean, also using 40 vertical levels but a tri-polar oceanic grid (see Figure 3) with two northern poles in Canada and Siberia and a third pole at the South Pole [Giorgetta *et al.*, 2013].

The atmospheric model ECHAM6 of MPI-ESM-LR uses a T63/ 1.9° horizontal resolution with 47 vertical levels. MR uses the same horizontal resolution, but with a higher (95 levels) vertical resolution.

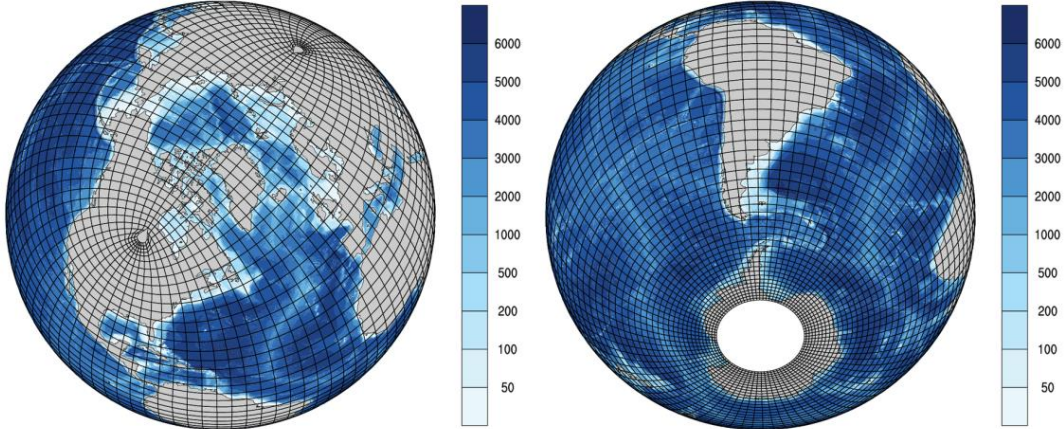


Figure 3. Tri-polar MPIOM-grid used in the MPI-ESM-MR simulations. Illustration of the two North Poles (left) and the South Pole (right). The land is represented by the grey areas, the ocean and its depth by the blue shades.

3.1.2. MPI-ESM Sea-ice Module

Sea-ice in the MPI-ESM is represented by the atmospheric module ECHAM6 and the ocean module MPIOM. The full sea-ice submodel within MPIOM simulates the sea-ice thickness and its dynamics. The thermodynamic part of the submodel contains minor changes compared to the predecessor model ECHAM5/MPIOM. The dynamics is based on a viscous-plastic ice rheology that defines the relationship between ice deformation and ice internal stress [Hibler, 1979]. The temperature at the sea-ice surface is calculated by the balance of incoming atmospheric fluxes, outgoing longwave radiation and the conductive heat through

the ice. The excess energy melts the ice, when the surface temperature exceeds 0°C. The accrued melt water is assigned to the uppermost ocean grid cell. The changes in heat transfer through the ice and snow represents the snow accumulation.

The ice-ocean heat exchange is represented by a simple balance between the oceanic heat flux and a conductive heat flux through ice, which changes the sea-ice thickness at its bottom. If there is any sea-ice present in an oceanic grid cell, the uppermost cell is kept at freezing temperature.

A lower boundary for fluxes between surface and atmosphere is provided by the atmospheric model ECHAM6. The calculation of the sea-ice surface temperature in this model is based on the surface albedo, the conductive heat flux through ice and snow, the incoming atmospheric fluxes and outgoing longwave radiation [Notz *et al.*, 2013].

The main improvement of sea-ice with respect to the prior ECHAM5/MPIOM is the consideration of the melt-ponds scheme in the albedo calculations [Notz *et al.*, 2013].

3.2. Model Simulations

Several long-term simulations have been performed with the MPI-ESM following the CMIP5 protocol [Taylor *et al.*, 2012].

The MPI-ESM-LR and -MR simulations analyzed in this work are part of the CMIP5 ensemble. CMIP provides a standard experimental protocol for studying the output of Earth system models and a community-based infrastructure in support of climate model analysis. The CMIP5 simulations that were ran by more than 20 different model centers have been carried out in support of the IPCC Fifth Assessment Report. Since the third phase of CMIP (CMIP3), the participating models have been further developed, new models have joined, and new emission scenarios, so-called Representative Concentration Pathways (RCPs) have been established [Moss *et al.*, 2010; Meinshausen *et al.*, 2011].

In this work, the CMIP5 historical (1850-2005) and future simulations under three different RCPs (2006-2100) are analyzed for three ensemble members of the MPI-ESM-LR configuration and three ensemble members of the MPI-ESM-MR configuration. Different ensemble members use different initial conditions [Blanchard-Wrigglesworth *et al.*, 2011]. The time series of different greenhouse gas concentrations are shown in Figure 4. CO₂ concentrations increase in all except the RCP 2.6 scenario and range from about 420 ppm in RCP 2.6 to about 935 ppm in RCP 8.5 in 2100, while nitrous oxide (N₂O) concentrations range from 345 to 435 ppm, respectively. Methane (CH₄) concentrations increase substantially above today's values (~1750 ppb) to more than 3500 ppb by 2100 in RCP 8.5, while in RCP 4.5 and RCP 6.0 CH₄ concentrations in 2100 are similar to today's values and decrease to ~1250 ppb in the RCP 2.6 scenario.

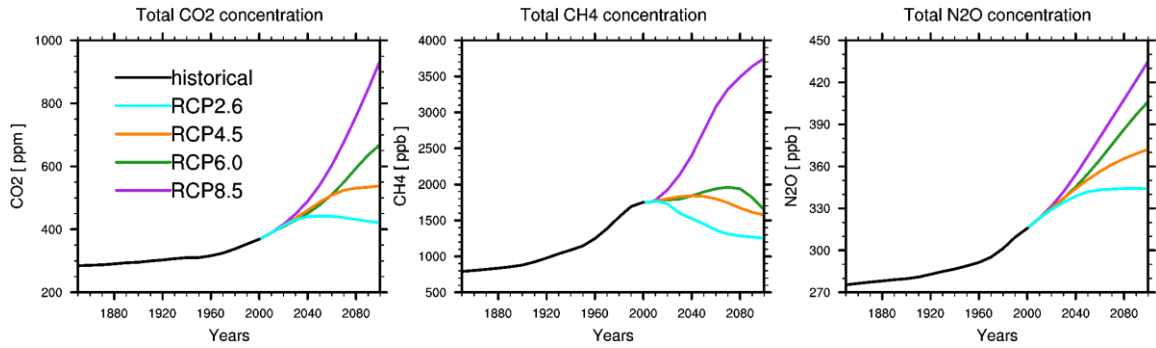


Figure 4. Time series of different greenhouse gas concentrations for (a) CO₂, (b) CH₄ and (c) N₂O in the historical period (1850 to 2000) and for the four RCPs (2000 to 2100).

The historical simulation is forced by natural and anthropogenic forcings that are derived from observations. In these simulations the spectral solar irradiance variability, Earth's orbit variations, seasonally tropospheric aerosol variation and also stratospheric aerosols from volcanic eruptions are considered as natural effects. Well mixed tropospheric greenhouse gases (e.g. CO₂, CH₄ and N₂O), ozone, seasonally and spatially resolved sulfate aerosols, land use and the carbon cycle are considered as anthropogenic forcing. The future is represented by the Representative Concentration Pathway (RCP) scenarios, which start when the historical experiment ends (2005), continue to 2100 and include the same natural forcings that are used in the historical simulations. MPI-ESM was ran for RCP 2.6 [*van Vuuren et al.*, 2011], RCP 4.5 [*Thomson et al.*, 2011] and RCP 8.5 [*Riahi et al.*, 2011], with different assumptions for anthropogenic forcing that lead to different global warming ranges. The RCP 2.6 simulation in the MPI-ESM corresponds to a global warming of around 1.5°C from 1850 to 2100, while the RCP 8.5 scenario projects a warming of around 4.8°C over the same period [*Giorgetta et al.*, 2013].

4. Sea-ice Observations for Model Evaluation

The sea-ice observational data used in this work are based on different sources which are briefly described in this Chapter. The simulated sea-ice extent is compared to the AMSR-E dataset [Spreen *et al.*, 2008], NSIDC data [Cavalieri *et al.*, 1997] and the Hadley Centre Sea Ice and Sea Surface Temperature (HadISST, Rayner *et al.* [2003]) dataset.

4.1. Sea-ice Observations

4.1.1. Measurement Techniques and Retrieval

The Arctic and Antarctic sea-ice is well observed since the late 1970s, when the first satellite instruments became available. Satellite observations of sea-ice are mostly based on microwave radiometers. These instruments measure the microwave radiation emitted by the Earth, typically in the frequency range of 6.9 -89 GHz (AMSR-E, Spreen *et al.* [2008]). By assuming a specific emissivity, it is possible to reconstruct the emission spectrum of the observed radiation and to relate it to a corresponding (brightness) temperature [Spencer, 2001]. The NSIDC and AMSR-E observational datasets used in this work were generated by different types of satellite-based passive microwave radiometers (see Sections 4.1.2 and 4.1.3).

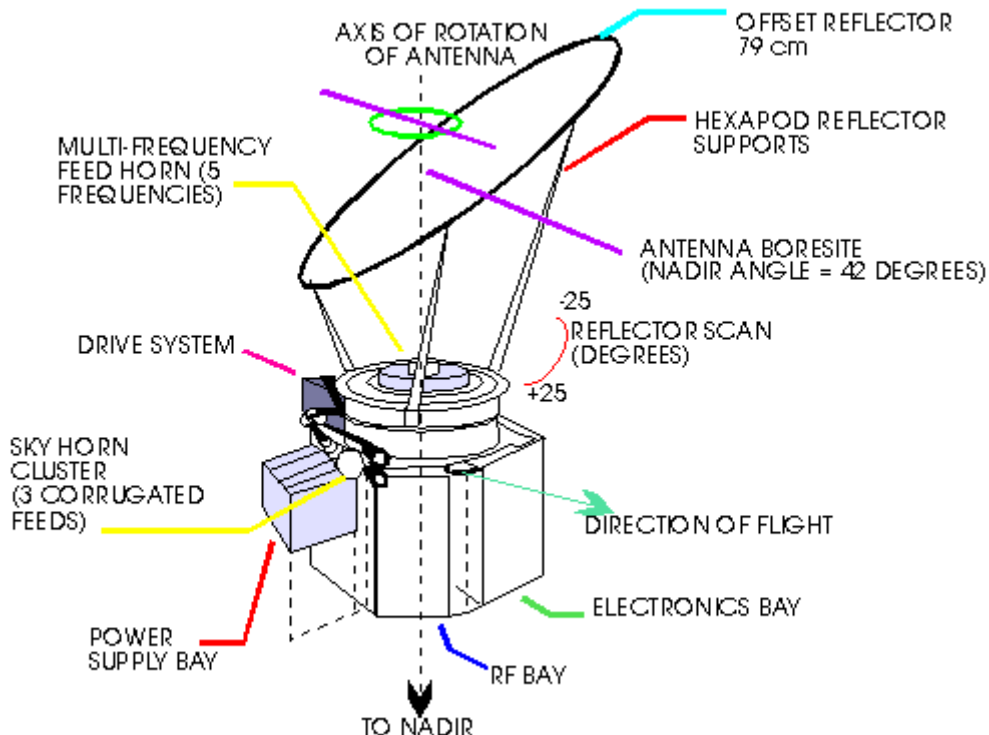


Figure 5. Nimbus-7 Scanning Multichannel Microwave Radiometer (SMMR) Setup [Gloersen and Hardis, 1978]

The sea-ice concentration is then obtained by using complex algorithms that interpret the measured temperatures in terms of emission. Unfrozen open water surface emits a small amount of polarized microwave radiation. More microwaves but less polarized are emitted by first year ice. The signature of multiyear sea-ice is between open water and first year ice [Meier, 2012]. The NSIDC dataset is derived from two different algorithms, the NASA Team algorithm and the Bootstrap algorithm [Comiso *et al.*, 1997]. While the latter is based on interpolation between clusters of pure ice types, the NASA Team algorithm uses the ratios of brightness temperatures. Employing a land-sea mask, the ice ashore can be precluded and the sea-ice concentration remains.

The advantages of this measuring method are that microwave radiation can penetrate clouds, the measure is independent from solar radiation and thus also works at polar night, and that daily datasets can be provided for long term observations.

4.1.2. AMSR-E

The Advanced Microwave Scanning Radiometer - Earth Observing System (AMSR-E) instrument has a horizontal resolution of approximately 6×4 km at 89 GHz. This is nearly three times the spatial resolution of the Special Sensor Microwave/Imager (SSM/I) sensor, used for measuring the NSIDC data, at 85 GHz, which has 15×13 km [Spreen *et al.*, 2008]. The instrument was launched on May 4th, 2002 aboard the NASA Earth Observing System (EOS) Aqua Satellite. It is a passive-microwave radiometer system and provides twelve channels, six frequencies and scans conically. With a frequency range from 6.9 GHz to 89 GHz it measures the brightness temperatures through both horizontally and vertically polarized microwave radiation. The National Space Development Agency of Japan (NASDA), now renamed to Japan Aerospace Exploration Agency (JAXA), developed AMSR-E and AMSR, which was lost in October 2003.

For the investigation of global energy and water cycles, the AMSR-E instrument provides measurements of oceanic, land and atmospheric parameters. It measures precipitation rate, atmospheric cloud water, water vapor, surface wetness, sea surface temperature, wind speed and sea- ice concentrations. The sea-ice concentration that is derived by the algorithms of the widespread NASA-Team and Bootstrap algorithms [Emery *et al.*, 1994], is gathered by the channels with the coarsest resolution, i.e. the 19 and 37 GHz channels. These also have a higher spatial resolution, more than three times of the standard SSM/I sensors respective channels.

The AMSR-E sea-ice concentration dataset used in this work was provided by the Institute of Environmental Physics at the University of Bremen. In this dataset the Level A1 data of both 89 GHz channels is used. The lower channels are used for validation purposes and as weather filters for spurious ice detection in the open ocean. The ARTIST Sea Ice (ASI) algorithm was used for the Bremen AMSR-E dataset. ARTIST stands for Arctic Radiation and Turbulence

Interaction Study, a research project around Svalbard, Norway, in 1998 [Hartmann *et al.*, 1999]. The provided dataset covers a period from July 2002 to August 2011. It is provided as dataset mapped onto the NSIDC grid.

As an example, Figure 6 shows the sea-ice extent over the Arctic (left) and Antarctic (right) in 2005 for September (upper row) and March (lower row), as observed by AMSR-E.

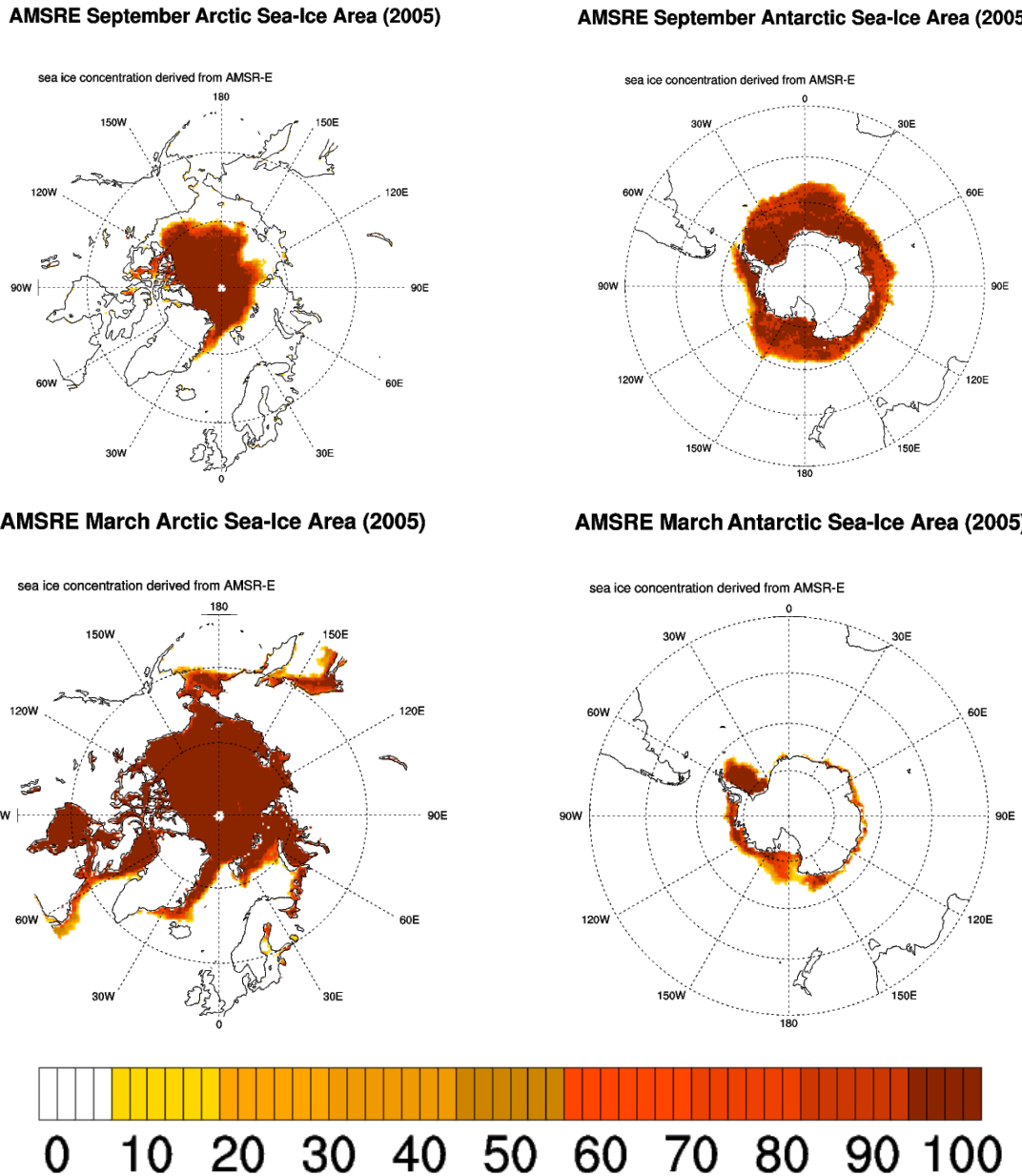


Figure 6. Polar stereographic projection of Arctic (left) and Antarctic (right) September (1st row) and March (2nd row) sea-ice concentration [%] derived from the AMSR-E measurements in 2005

4.1.3. NSIDC

The sea-ice concentration dataset provided by the National Snow and Ice Data Center (NSIDC) includes gridded daily and monthly averaged sea-ice concentrations [Fetterer *et al.*, 2002]. The data used for this work were downloaded from <http://nsidc.org/data/nsidc-0051.html>. The data are depicted in a polar stereographic projection at a grid cell resolution of 25 km, and starts on 26 October 1978. The dataset is based on the brightness temperature data detected from multiple sensors. The instruments used are the Nimbus-7 Scanning Multichannel Microwave Radiometer (SMMR), the Defense Meteorological Satellite Program (DMSP) -F8, -F11 and -F13 SSM/I_s, and the DMSP-F17 Special Sensor Microwave Imager/Sounder (SSMIS). Due to inclination of the platform orbits, the measurements cover an area up to 87.2°N latitude.

To improve the quality of the dataset the brightness temperatures is measured by sensors with different frequencies, the gathered data is mapped onto a common grid, a land mask is applied, the adjustment for land-to-ocean spillover and the remaining area differences between the sensors are reduced by inter-sensor corrections [Cavalieri *et al.*, 1999]. The sea-ice concentration of the dataset used in this work has been generated by the NASA Team algorithm [Documentation of Sea Ice Concentrations from Nimbus-7 SMMR and DMSP SSM/I-SSMIS Passive Microwave Data, http://nsidc.org/data/docs/daac/nsidc0051_gsfc_seaice.gd.html].

The minimization of the differences in the sea-ice extent and the ice covered area when transitioning to the next instrument, the so called overlap periods, is gained by “tuning” the algorithms. Due to orbital differences MMR and SSM/I-SSMIS have different data gaps at the North Pole. Consequently, each time series of parameters needs to take these distinctions into account. For this purpose a pole mask is provided. During the period when new sea-ice makes up a substantial part of the sea-ice cover and in summer when melt is present, deviations to the real sea-ice concentration occur. Due to weather effects and the mixing of ocean and land in the sensors field of view (FOV), some errors remain [Gloersen, 1983].

To calculate the sea-ice extent respectively the area from the sea-ice concentration, the NSIDC provides special area-files for each resolution and both hemispheres, which contain the area for each grid cell (see Section 4.2. Methodology). The sea-ice extent can then easily be calculated by multiplying the sea-ice concentration and the appropriate area file.

The NSIDC dataset covers the period from October 1978 to December 2011.

4.1.4. HadISST

The Hadley Centre Sea Ice and Sea Surface Temperature dataset (HadISST) is a combination of sea-ice concentration and monthly globally-complete fields of sea surface temperature (SST). The dataset covers the period from 1870 to the present [Rayner *et al.*, 2003]. Since 1981, the HadISST dataset have been improved by the satellite-borne advanced very high

resolution radiometer (AVHRR), which measures the reflectance of the Earth in 5 spectral bands. The form of these data, separately estimated for day and night, are 1° area monthly observations.

Since the HadISST observational data started before satellite based measurements were available, the sea-ice concentration was derived from the SSTs with thresholds that predict the occurrence of ice. The SST data, recorded from ships and buoys, of the HadISST are from the Met Office Marine Data Bank (MDB), additionally includes data from the Global Telecommunications System (GTS). Gaps in the SST dataset have been interpolated to complete HadISST.

The available HadISST observational data ranges from January 1870 to December 2008 and uses a land sea mask modified from ECHAM/MESSy Atmospheric Chemistry (*EMAC*) model. Here we start from the time of the satellite-based observations, therefore we consider the period from 1982 to 2008.

4.2. Methodology

The plots presented in this work are produced using the NCAR Command Language (NCL), a programming language especially designed for the analysis and visualization of geo-based scientific data, also providing several built-in functions. NCL is a free interpreted language and was developed by the National Center for Atmospheric Research (NCAR).

All the input datasets, model data and observation data, are in the network Common Data Form (netCDF) format, which can store multidimensional data.

Sea-ice data are provided as sea-ice concentrations C on each point of the grid, ranging from 0 to 100%. This is then normalized to a [0-1] range, with 0 and 1 representing an ice-free and fully ice-covered grid cell, respectively. Land surface values (available in some dataset) are assumed to be zero. To convert from sea-ice concentration to sea-ice area S , the concentration needs to be multiplied by the area element dA of each cell of the grid:

$$S(\theta, \varphi) = C(\theta, \varphi) * dA(\theta, \varphi),$$

at each latitude and longitude position (θ, φ) .

The input data uses different grid types. The HadISST dataset is based on a regular grid, for which the area element dA can be calculated as the standard area element on the sphere:

$$dA(\theta, \varphi) = R^2 \sin \varphi d\varphi d\theta,$$

with R being the Earth's radius. For irregular grids (like NSIDC, AMSR-E and MPI-ESM) the calculation of the area element is more complicated and the area fields provided by each dataset together with the sea-ice concentration data were used. To maintain the resolution

of the original datasets, we refrain from performing a re-gridding of the data, which are therefore shown on their native grids.

For a better comparability of model and observations, the sea-ice area is converted to extent. Therefore grid cells with an ice concentration larger or equal than 15% are counted as completely covered and the concentration is set to 1.

To obtain the sea-ice extent E in each hemisphere, the sea-ice area is summed over all grid cells of that hemisphere:

$$E = \sum \theta \sum \varphi S(\theta, \varphi), \text{ respectively } E = \sum x \sum y S(x, y),$$

for irregular grids, with the grid cell variables (x, y) .

Concerning the area of the grid cells close to the Poles, which is not covered by the satellite observations due to orbit constraints, the respective missing areas were added to the measured data. The corresponding area element was calculated using the maximum latitude φ_{\max} of the given dataset:

$$dA = 2\pi R^2 (1 - \sin \varphi_{\max}).$$

5. Results

This Chapter summarizes the results that have been achieved in this work for the Arctic (Section 5.1) and for the Antarctic (Section 5.2). Each of these sections first presents the sea-ice comparison of the MPI-ESM to the observational datasets of NSIDC, AMSR-E and HadISST before analyzing future sea-ice projections in a second step.

5.1. Arctic Sea-ice

Due to the geographical conditions, the sea-ice of the Northern Hemisphere is especially influenced by global warming [*Lingenhöhl*, 2012]. In addition, *Stroeve et al.* [2007] found that the CMIP3 model ensemble underestimates observed September sea-ice trend over the last decade. Consequently, a lot of the attention of the scientific community is currently focusing on Arctic sea-ice [*Kattsov et al.*, 2010].

5.1.1. Evaluation of sea-ice in the Arctic

Figure 7 shows the timeseries of the September mean Arctic sea-ice extent from 1980 to 2011 as simulated by the MPI-ESM compared to observations. Sea-ice extent is shown in units of million square kilometers. The light green and blue lines show the three ensemble members of MPI-ESM-LR and MPI-ESM-MR, while the darker and thicker green and blue lines show the mean over the three ensemble members, respectively. The observational datasets are illustrated by the dark red (NSIDC), yellow (HadISST) and purple (AMSR-E) lines.

The large inter-annual variability that can be seen in the observations is also present in the different MPI-ESM ensemble members, which reproduce well the range of the observational data. Thus, even if no single ensemble member exactly matches the observational data, the group of ensemble members is capable to reproduce the shape. The interannual variability of MPI-ESM is discussed in detail in *Notz et al.* [2013].

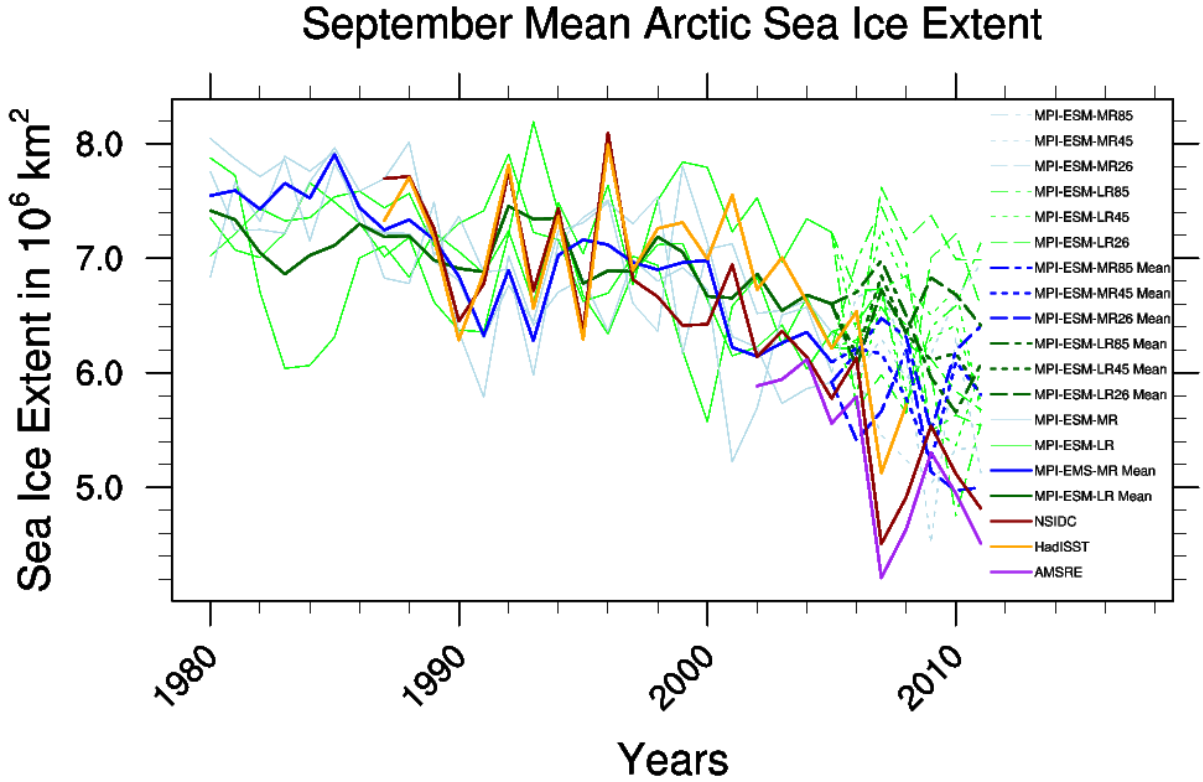


Figure 7. Timeseries (1980-2011) of September Arctic sea-ice extent from the CMIP5 MPI-ESM-LR (green) and MPI-ESM-MR (blue) historical simulations (1850-2005) compared to observations: NSIDC (1987-2011, dark red), HadISST (1987-2011, orange), and AMSR-E (2002-2011, purple). Sea-ice extent is calculated as the total area of grid cells with a sea-ice concentrations of at least 15%. Each thin colored line represents one ensemble member and the thick colored lines the ensemble mean of all members for each model version.

To further evaluate the MPI-ESM, the seasonal cycle of climatologic mean (monthly mean) Arctic sea-ice extent is shown in Figure 8. The upper panel shows a mean over 1982-2002, while the lower panel shows a mean over the period 2003-2008. In the upper panel only the HadISST and NSIDC datasets are used for comparison, since the AMSR-E data do not cover this time period. The period from 2003 to 2008 has been chosen because this is the only time period where data from all three observations is available.

Similar to Figure 7, both the individual MPI-ESM ensemble members and the ensemble means are shown. Overall this figure demonstrates that the seasonal cycle and the absolute magnitude of sea-ice extent in the Arctic is very well represented in the MPI-ESM. Only during winter the sea-ice extent is slightly smaller in MPI-ESM than in both observations. Overall the HadISST dataset shows a slightly larger sea-ice extent during the whole cycle in both periods.

While the model ensemble members in the upper panel have a low variance, their deviation in the annual cycle from 2003 to 2008 is exceeded, especially during the Arctic summer. The AMSR-E data represent a cycle similar to the NSIDC data, but with a smaller extent during the Arctic winter. In this season the observations deviate most from each other.

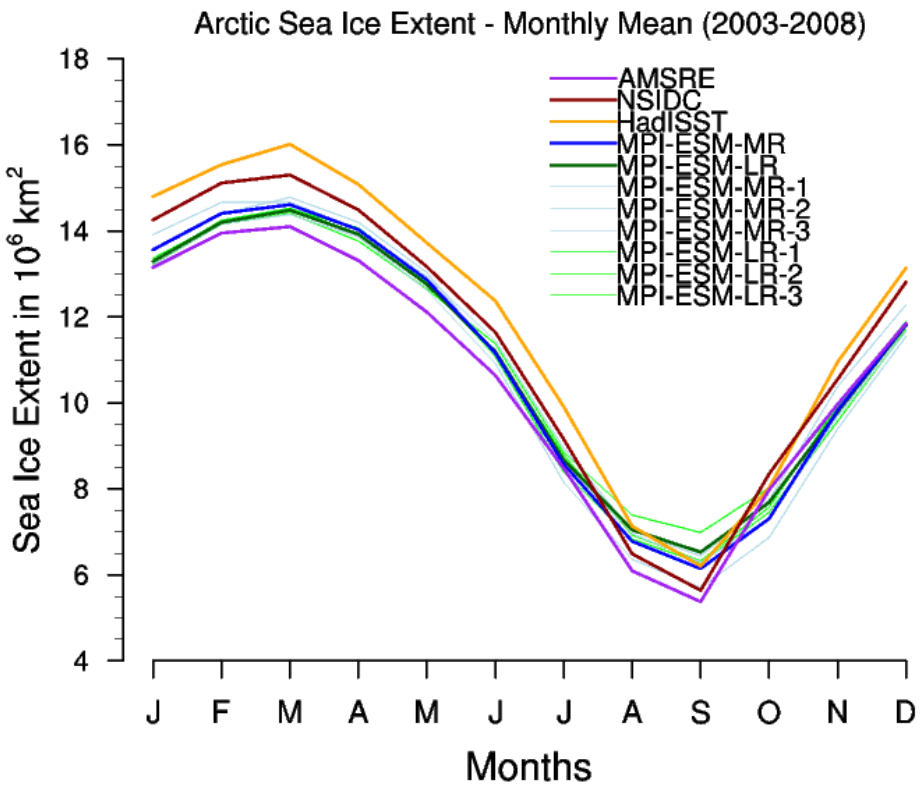
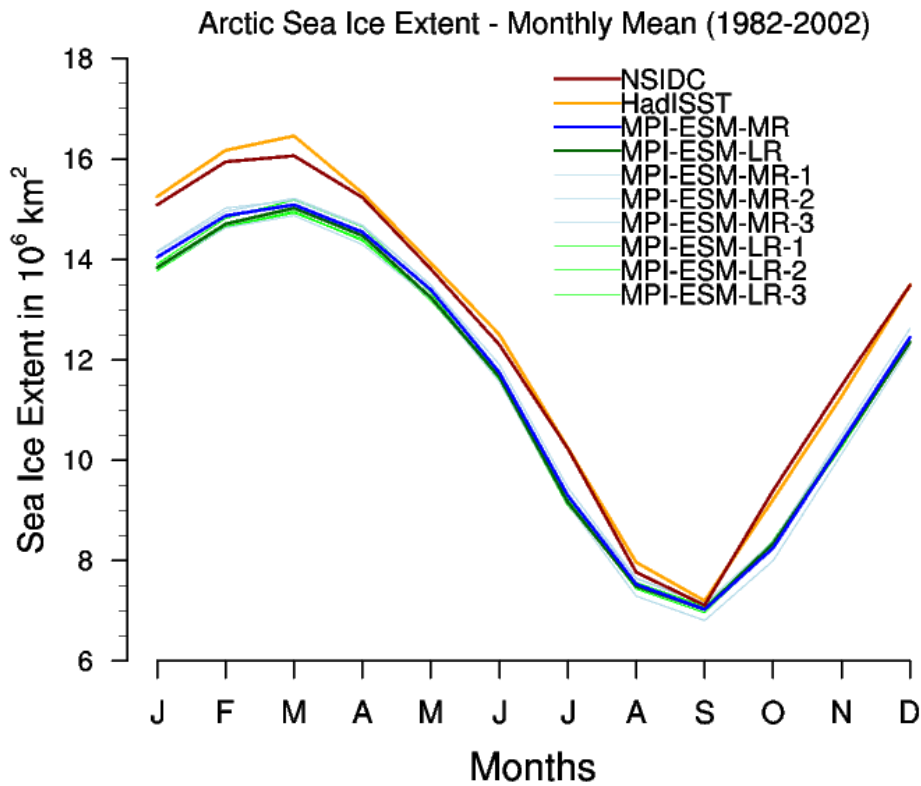


Figure 8. Mean seasonal cycle in sea-ice extent in the Northern Hemisphere averaged over 1982-2002 (upper panel) and 2003-2008 (lower panel, using RCP 4.5 for 2006-2008) as simulated by the CMIP5 MPI-ESM-LR (green) and MPI-ESM-MR (blue) models compared to observations. Each thin colored line represents one ensemble member and the thick colored lines the ensemble mean of all members for each model version. The thick purple, dark red and orange lines show observations from AMSR-E (lower panel only) NSIDC and HadISST, respectively.

The geographical distribution of the September climatological mean (2003-2008) sea-ice extent over the Arctic from the MPI-ESM compared to observations is depicted in Figure 9. This figure shows the MPI-ESM-LR (first row) and the MPI-ESM-MR (second row) simulations for each individual ensemble member (first to third column), and the ensemble mean (fourth column). The last row shows the observations NSIDC (first column), AMSR-E (second column) and the HadISST dataset (third column). The MPI-ESM spatial pattern of the sea-ice cover is in good agreement with the observations. A nearly full ice-covered area north of 80°N latitude (north of Iceland) is simulated by the MPI-ESM, in agreement with the observations.

A similar good performance is found for the sea-ice at the east coast of Greenland and at the Queen Elizabeth Islands. The total ice area in the model is slightly larger than observed, especially over Laptev Sea, East Siberian Sea, Chukchi Sea and Beaufort Sea. The single ensemble members show a comparable distribution with some differences at the Laptev Sea, the Siberian cost line, the Beaufort Sea and around the North Pole.

The patterns of the simulated sea-ice are overall in excellent agreement with observations, although the AMSR-E data depicts a higher sea-ice concentration in the polar region and the HadISST data shows some more ice at the Siberian coast.

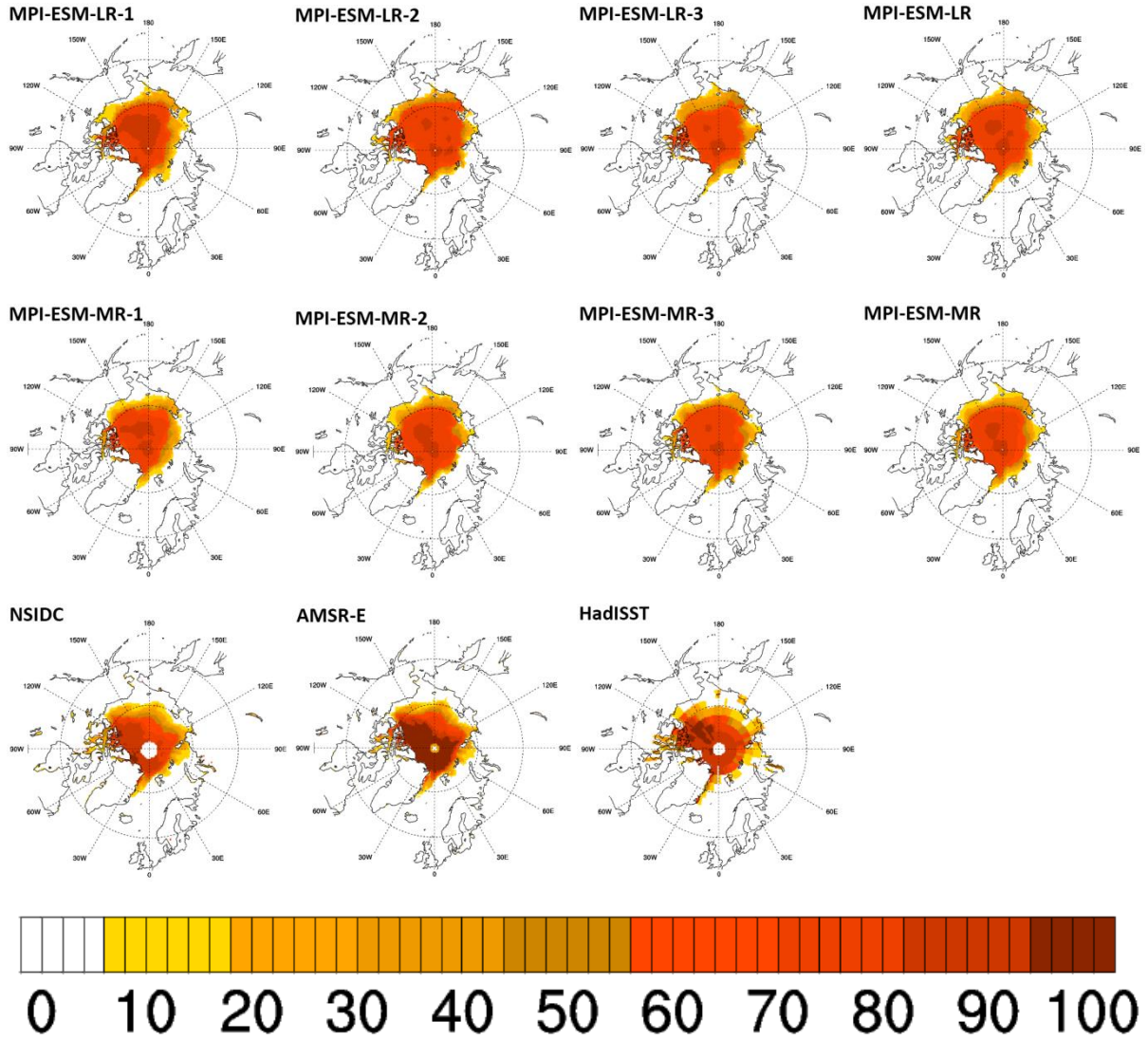


Figure 9. Polar stereographic projection of mean Arctic September sea-ice concentrations [%] averaged over the period 2003-2008 as simulated by the individual ensemble members (first to third column) and the ensemble mean (fourth column) of MPI-ESM-LR (first row) and MPI-ESM-MR (second row) compared to observations from NSIDC, AMSR-E and HadISST (third row).

5.1.2. September Arctic sea-ice Projections

Overall, the evaluation of Arctic sea-ice in Section 5.1.1 reveals that the MPI-ESM is well able to reproduce observed sea-ice distributions and trends in the Northern Hemisphere. The CMIP5 MPI-ESM model simulations [Giorgetta *et al.*, 2013] are therefore now analyzed to study how summer-time Arctic sea ice is projected to change over the 21st century under different scenarios.

Figure 10 shows the timeseries of September Arctic sea-ice from 1850 to 2100. The figure is based on the MPI-ESM historical simulations (1850-2005) and the three RCP simulations (2006-2100). The different RCP simulations are shown in blue (RCP 2.6), light blue (RCP 4.5) and red (RCP 8.5).

In the RCP2.6 simulation a further decrease of summer-time Arctic sea-ice until around 2050 is projected. Afterwards, the decline stops and the sea-ice extent stabilizes at around 5 million square kilometers during the second half of the 21st century. In the MPI-ESM RCP 8.5 simulation however, a strong loss of summer-time Arctic sea-ice is projected during the 21st century. Under the RCP 8.5 scenario, the MPI-ESM model simulates an ice free summer during the second half of the 21st century [see also Notz *et al.*, 2013].

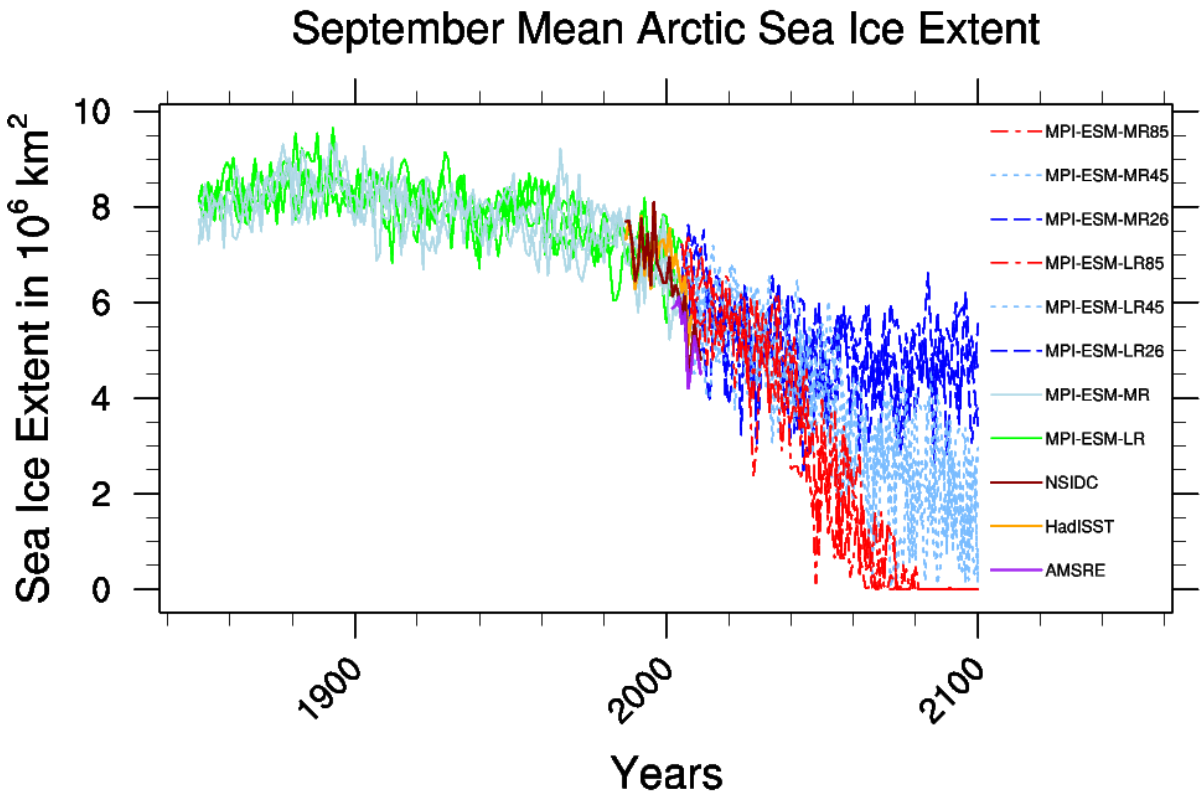


Figure 10. Same as Figure 7 but for the time period 1850-2100. The MPI-ESM historical simulations are extended with simulations under the RCP 2.5 (blue), 4.5 (light blue) and 8.5 (red).

This is further illustrated in the polar stereographic projections in Figure 11, which compares the geographical distribution of the 20 year mean historical MPI-ESM simulation from 1980-2000 (first column) to the mean from 2030-2050 (second column) and 2080-2100 (third column) in the three RCP simulations. In each of the panels the average over all three ensemble members is shown. The scenarios RCP 2.6, RCP 4.5 and RCP 8.5 are illustrated in the first, second and third row respectively (with the first panel always showing the historical period)

The RCP 2.6 simulation projects a further decrease of the sea-ice cover, apparent at the projections from 1980-2000 in comparison to 2030-2050 with a decreasing concentration and ice-loss around the Russian, American and Canadian coast line. The mean area from 2080-2100 projects a stabilization of the Arctic ice during the second half of the 21st century. The second row shows a further melting under the RCP 4.5 scenario during the 21st century. Thus the second plot shows a sea-ice decline, comparable to the RCP 2.6 scenario. The 2080-

2100 mean predicts a further ice loss and a small area of higher sea-ice concentration around the 150°W longitude/95°N latitude region. The most dramatic scenario is illustrated in the last row by the RCP 8.5 simulation. The 2030-2050 mean predicts already a strong decrease of sea-ice with an area of higher ice concentration north of the Ellesmere Island. The mean sea-ice concentration from 2080 to 2100 exhibits an ice-free Arctic summer (see also Figure 10).

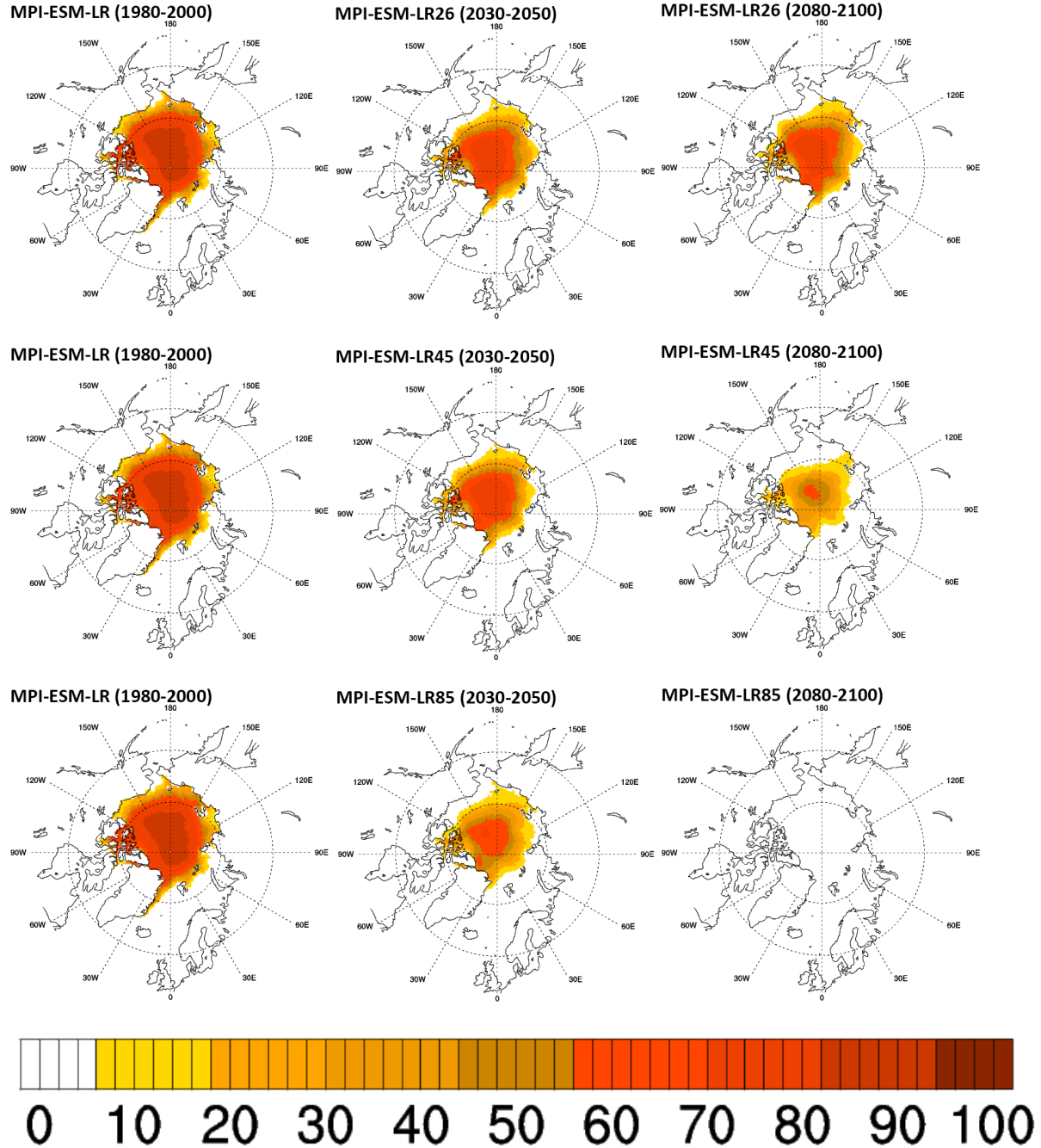


Figure 11. Polar stereographic projection of the 20-year mean Arctic September sea-ice area under the different RCP future scenarios - RCP 2.6 (first row), RCP 4.5 (second row) and RCP 8.5 (third row). The first column shows the historical simulation (1980-2000) in each row. The second column shows the RCP means in the period from 2030 to 2050 and the third column from 2080 to 2100, respectively.

5.2. Antarctic sea-ice

The sea-ice extent over Antarctica is much smaller than in the Arctic. According to the observations, in the year 2000 the minimum Antarctic value was about 4 million square kilometers, versus a value of 7 million square kilometers for the Arctic and the trend is also smaller [*Cavalieri and Parkinson, 2008*].

5.2.1. Evaluation of sea-ice in the Antarctic

To evaluate the MPI-ESM in the Antarctic, Figure 12 shows the annual mean timeseries of sea-ice extent from 1980 to 2011 over Antarctic in summer (March). The observational data are again represented in dark red (NSIDC), yellow (HadISST) and purple (AMSR-E). The MPI-ESM mean is plotted in green (MPI-ESM-MR) and blue (MPI-ESM-LR), with each three ensemble members as lighter and thinner lines. The March sea-ice extent is given in units of million square kilometers.

The observations show a large interannual variability of the sea-ice extent. This variability is also present in the ensemble members of MPI-ESM. A small trend is simulated over the period 1980-2011 in agreement with the observations. The NSIDC and the AMSR-E data values are very close to each other, while the HadISST dataset shows a similar trend, but with a small positive offset of around 0.9 million square kilometers (19%). In general, the model data dramatically underestimates the minimum sea-ice extent of about 3.6 million square kilometers (factor 3.77). This may be caused by a warm bias of the ocean temperature along the Antarctic coast (see Figure 15).

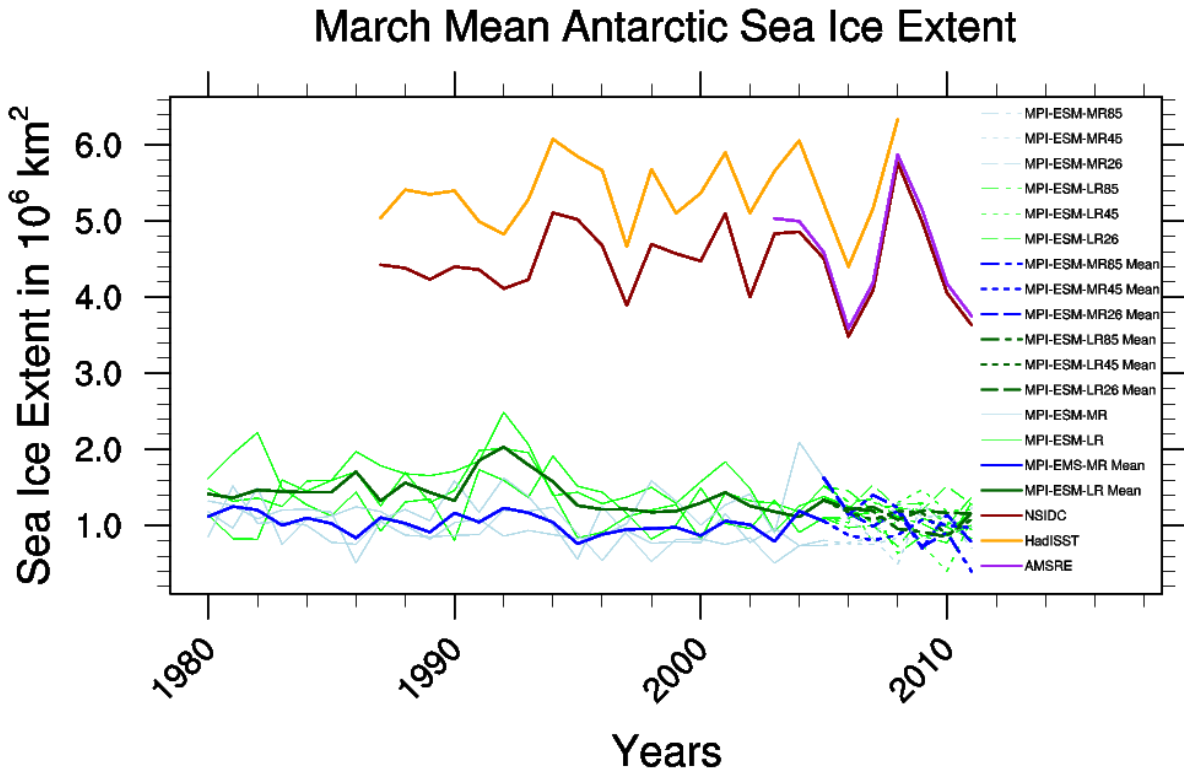


Figure 12. Timeseries from 1980 to 2011 of March Antarctic Sea-Ice extent from the CMIP5 MPI-ESM-LR (green) and MPI-ESM-MR (blue) historical simulations (1850-2005) compared to observations: NSIDC (1987-2011, dark red), HadISST (1987-2011, orange), and AMSR-E (2002-2011, purple). Sea-ice extent is calculated as the total area of grid cells with sea-ice concentrations of at least 15%. Each thin colored line represents one ensemble member and the thick colored lines the ensemble mean of all members for each model version.

The seasonal cycle of the climatological mean monthly mean sea-ice extent is shown in Figure 13 for 1982-2002 (upper panel) and for 2003-2008 (lower panel). The latter period also includes the AMSR-E dataset. The observations here are represented by AMSR-E (purple, lower panel only), NSIDC (dark red) and HadISST (yellow). The model means, MPI-ESM-LR (blue) and MPI-ESM-MR (green), and the single ensemble members (light blue and light green) are shown.

This figure demonstrates that the seasonal cycle is very well represented by the MPI-ESM, but again shows that the March Antarctic sea-ice extent is severely underestimated with respect to observations (see also Figure 12). The minimum in February/March is a little sharper than in the model data and on the other hand the maximum in September is less sharp than calculated by MPI-ESM. The different ensemble members of the MPI-ESM-LR and MPI-ESM-MR show relatively large differences among each other in Antarctic Winter in the 2003-2008 period. This is probably due to the short period with differences dominated by interannual variability.

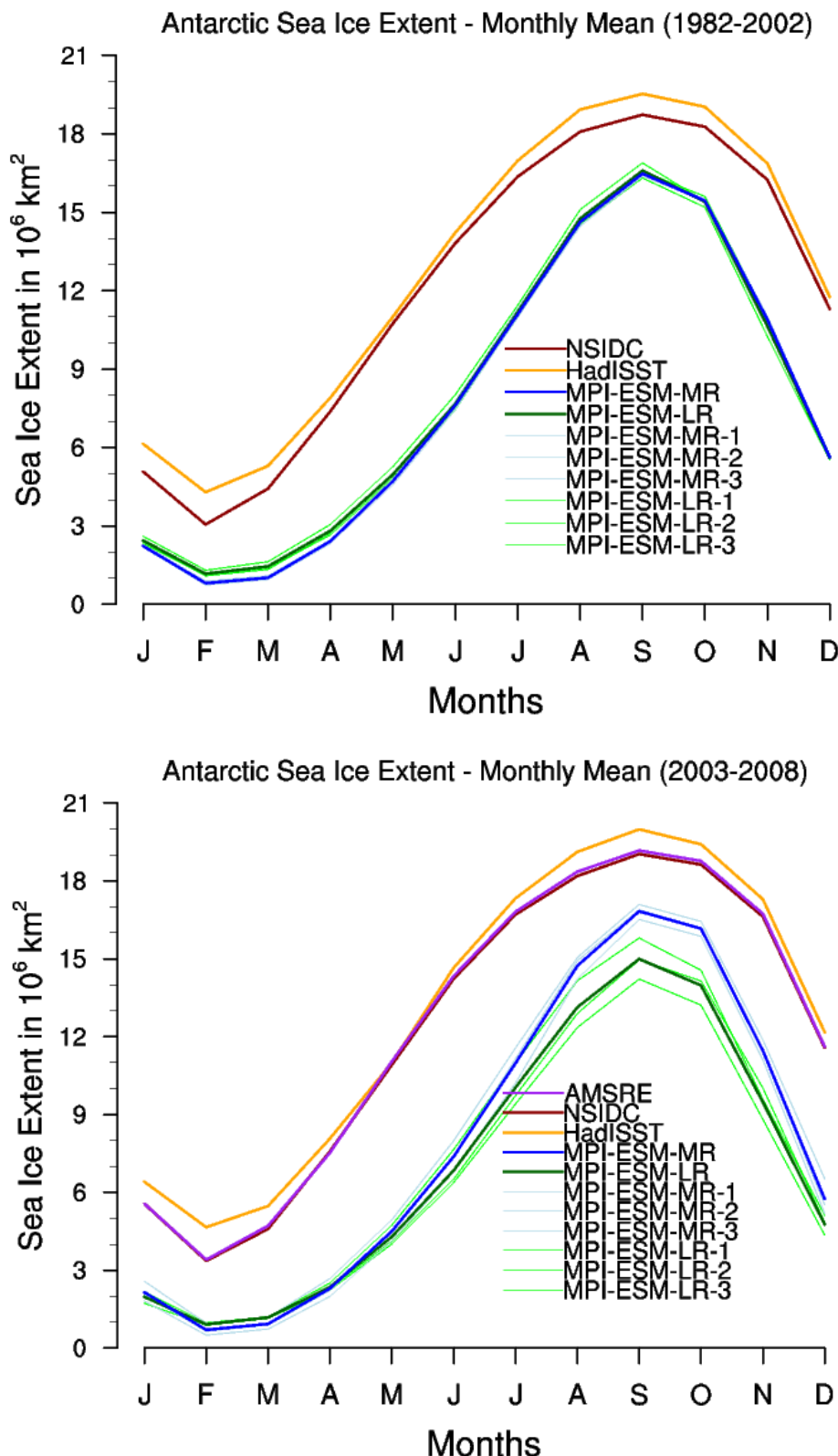


Figure 13. Mean seasonal cycle in sea-ice extent in the Southern Hemisphere averaged over 1982-2002 (upper panel) and 2003-2008 (lower panel, RCP45 for projection) as simulated by the CMIP5 MPI-ESM-LR (green) and MPI-ESM-MR (blue) models compared to observations. Each thin colored line represents one ensemble member and the thick colored lines the ensemble mean of all members for each model version. The thick purple, dark red and orange lines show observations from AMSR-E (lower panel only), NSIDC and HadISST, respectively.

Figure 14 illustrates the modeled geographical distributions of the Antarctic March climatological mean in comparison to the observations as polar stereographic projections for the period 2003-2008. The figure contains the MPI-ESM-LR (first row) and the MPI-ESM-MR (second row) simulations with their three ensemble members (first to third column) and the ensemble mean in the rightmost column. The last row shows the observational datasets from NSIDC (first column), AMSR-E (second column) and HadISST (third column).

The model simulations show a small ice cover with the highest concentration at the eastern Antarctic Peninsula, along the coastline of the Weddell Sea and of the Ross Sea.

As expected from the previous figures, the MPI-ESM underrates the observed sea-ice spread. When the established bias (see also Figure 14) in the simulations is fixed, a more robust conclusion can be drawn.

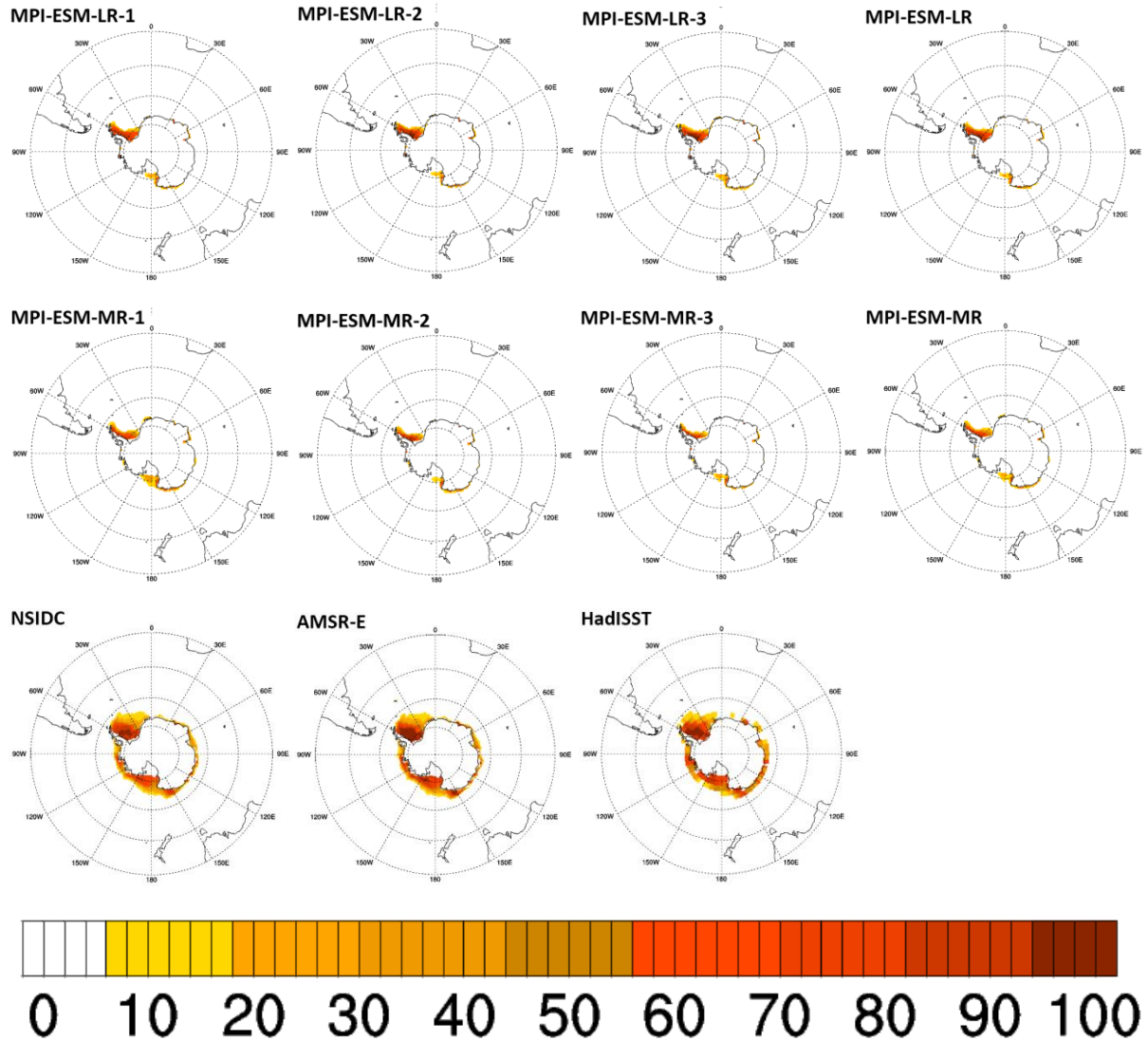


Figure 14. Polar stereographic Projection, mean Antarctic March sea-ice concentrations [%] averaged over the period 2003-2008 as simulated by the individual ensemble members (first to third column) and the ensemble mean(fourth row) of MPI-ESM-LR (first row) and MPI-ESM-MR (second row) compared to observations from NSIDC, AMSR-E and HadISST (third row).

One possible reason for the low bias of summer-time Antarctic sea-ice in the model is given in Figure 15. It shows a comparison of the mean sea surface temperature (SST) between HadISST (left panel) and the MPI-ESM (right panel) in March from 1982-2002. The SSTs are shown in Kelvin. The modeled SSTs in the Antarctic are slightly higher than in the HadISSTs dataset. This bias in SSTs is strongly influencing the formation of sea-ice in the MPI-ESM simulation and is a possible reason for the smaller sea-ice extent. The bias in SSTs has to be further examined in follow-up studies. Possible reasons for the observed cooler ocean temperatures are the rapid removal from surface-heat, which leads to a barely influence of the sea-ice cover, the katabatic outflow from the continent, that cools the near-surface layer, and a stratospheric cooling from springtime ozone depletion, that forces a colder climate over most of the coastlines [Stroeve *et al.*, 2007].

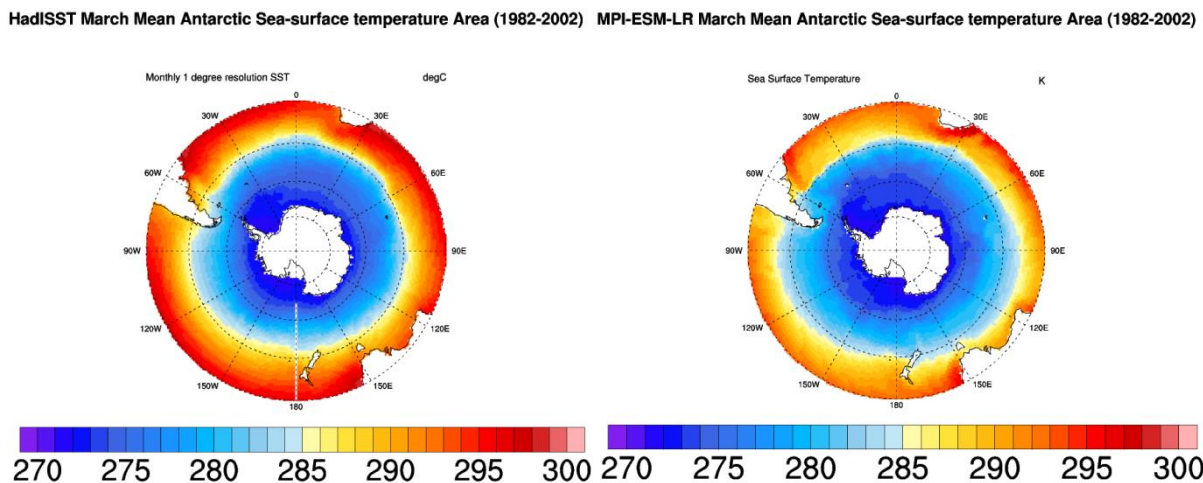


Figure 15. Mean Antarctic March sea surface temperatures [K] averaged over the period 1982-2002 as observed by HadISST (left panel) to the MPI-ESM-LR (right panel) simulations ensemble mean.

5.2.2. March Antarctic Sea-ice Projections

Since the MPI-ESM is able to simulate a realistic trend of the Antarctic sea-ice cover, in this section the future sea-ice projections for the 21st century will be investigated for different RCPs.

Figure 16 shows the timeseries of March Antarctic sea-ice extent from 1850 to 2100. Beside the MPI-ESM historical simulations (1850-2005), the three different RCPs are shown in blue (RCP 2.6), light blue (RCP 4.5) and red (RCP 8.5).

The historical model data and the future scenarios illustrate a large inter-annual variability, which is in agreement with the observations. The RCP 2.6 scenario shows a small decrease during the first half of the 21st century and an increase during the second half. In the RCP 8.5 simulation, a further decrease of the sea-ice cover with a possible ice-free summer at the end of the 21st century is projected.

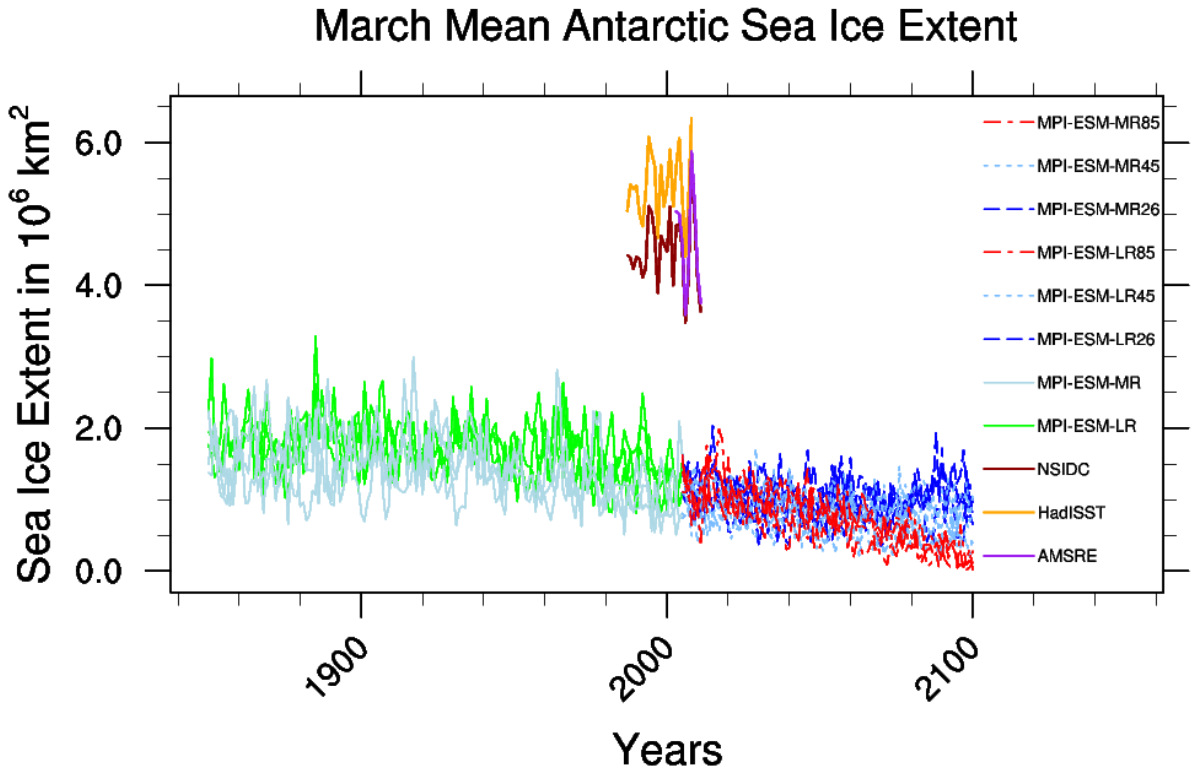


Figure 16. Same as Figure 12 but for the time period 1850-2100. The MPI-ESM historical simulations are extended with simulations under the RCP 2.5 (blue), 4.5 (light blue) and 8.5 (red).

The geographical distribution of the MPI-ESM projections are illustrated in Figure 17. The 20 year means of the MPI-ESM historical simulation from 1980-2000 (first column), and the mean future projections from 2030-2050 (second column) and 2080-2100 (third column) of Antarctic March sea-ice extent are plotted. The first column always shows the historical state and the RCPs are shown in the different rows (RCP 2.6, RCP 4.5 and RCP 8.5, from top to bottom). The calculated means are averaged over the respective three ensemble members for the historical and the RCP simulations.

As already shown in Figure 15, the Antarctic sea-ice cover trend is very small. However, the different RCP scenarios simulate recognizable trends. The RCP 2.6 simulation predicts a small decrease of the sea-ice cover at the eastern Arctic coastline, in the Weddel Sea and the Ross Sea from 1980-2000 to 2030-2050. The RCP 2.6 projection averaged over 2080-2100 shows a similar distribution with a little increase at the ice-edges. The positive trend in the second half of the 21st century, shown in Figure 16, is not that obvious in the geographical distribution. The RCP 4.5 scenario projects a larger decrease than in RCP 2.6. The decline also occurs at the eastern Antarctic coastline, in the Weddel Sea and the Ross Sea until 2030-2050. The RCP 4.5 2080-2100 mean shows a very similar sea-ice cover than the 2030-2050 mean. The largest sea-ice decrease is simulated in the RCP 8.5 scenario. The mean of 2030-2050 shows a similar decline to the other two projections. The 2080-2100 mean illustrates a further strong sea-ice decrease. The only ice left is a small sea-ice belt at the eastern Arctic Peninsula and ice floes in the Ross Sea. This scenario is close to an ice-free Antarctic summer.

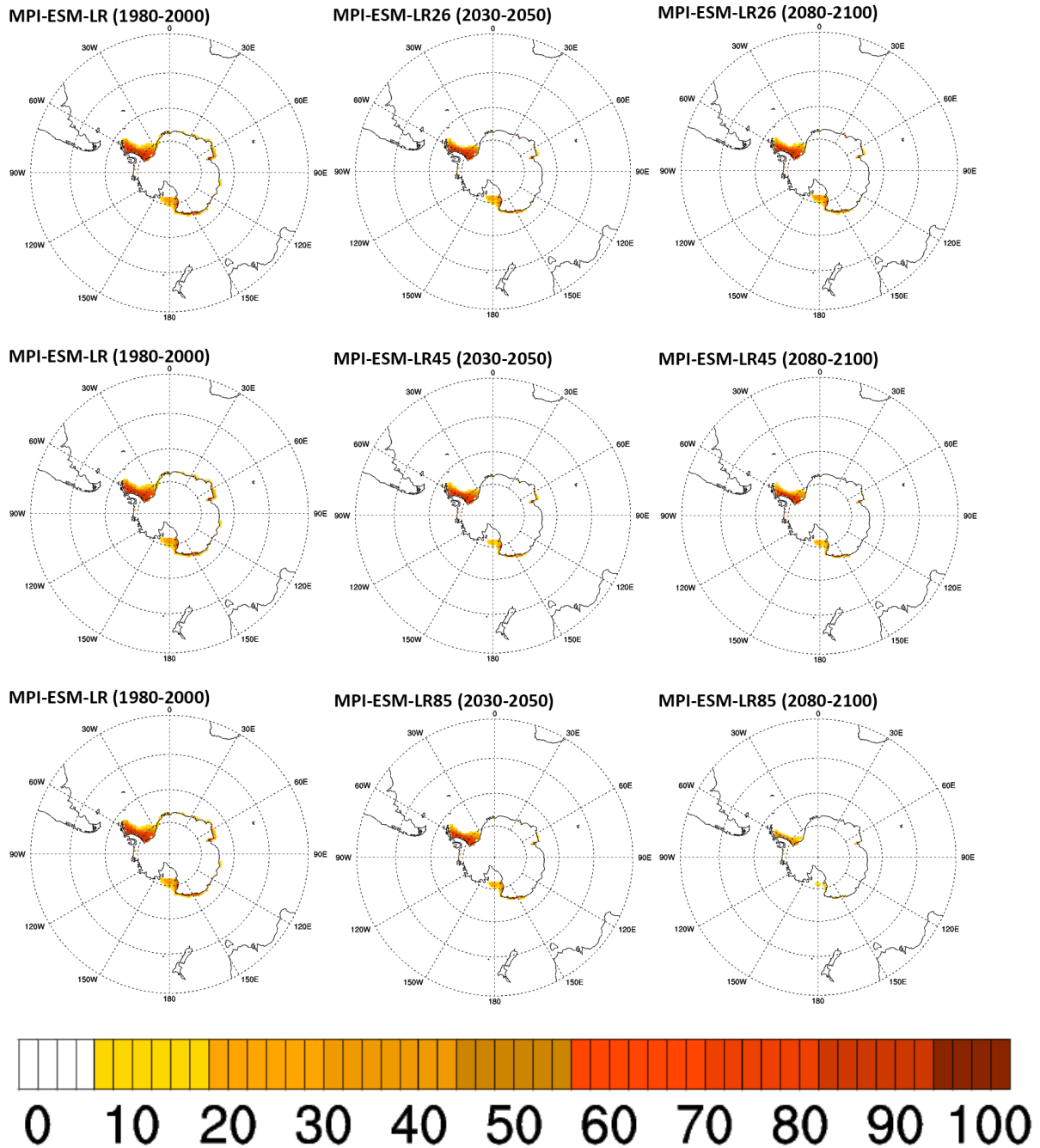


Figure 17. Polar stereographic projection of the 20-year mean Antarctic March sea-ice area under the different RCP future scenarios - RCP 2.6 (1st row), RCP 4.5 (2nd row) and RCP 8.5 (3rd row). The 1st column shows the historical simulation (1980-2000) each. The 2nd column shows the RCP means in the period from 2030 to 2050 and the 3rd column from 2080 to 2080 respectively.

6. Summary and Outlook

The goal of this work was to evaluate the sea-ice distribution in the Max Planck Institute Earth System Model (MPI-ESM) and to analyze the projections of sea-ice during the 21st century. For the sea-ice evaluation, the historical simulations were compared to three different observational datasets: the AMSR-E (Advanced Microwave Scanning Radiometer - Earth Observing System), NSIDC (National Snow and Ice Data Center) and HadISST (Hadley Centre Sea Ice and Sea Surface Temperature) datasets. All three datasets provide sea-ice concentrations and are given on different grids. In a first step the sea-ice area of each grid cell has been calculated from the sea-ice concentrations. For the regular latitude-longitude grid on which the HadISST dataset was provided, the grid cell area is calculated as the standard area element on the sphere. For irregular grids, area-files that were available for the NSIDC, AMSR-E and MPI-ESM data were used for this calculation. To ensure a better comparability, the sea-ice extent was used, thus grid cells with at least 15% coverage are assumed as totally covered. The total sea-ice extent is then the sum of the sea-ice area over all grid cells. The sea-ice distributions were evaluated separately for the Arctic and the Antarctic, with a focus on the seasonal cycle and summer-time trends.

In the Arctic, the historical MPI-ESM simulations (1850-2005) realistically represent the observed climatological mean seasonal cycle and also the spatial distribution of the Arctic sea-ice extent. The simulated September Arctic sea-ice extent is well simulated by the different ensemble members, with a realistic large internal interannual variability. The different Representative Concentration Pathway (RCP) simulations (2006-2100) provide future projections under different assumptions of future atmospheric carbon dioxide concentrations and other greenhouse gases. Under the RCP 2.6 scenario, an Arctic ice-free summer can still be avoided, while the RCP 8.5 projection simulates a strong sea-ice decrease and an ice-free summer during the second half of the 21st century.

The seasonal cycle of the climatological mean sea-ice extent over Antarctica is realistically simulated by the MPI-ESM, but the total amount is substantially underestimated. The observational datasets show relatively small trends in Antarctic summer-time sea-ice extent, which is in agreement with the model simulations. The RCP scenarios also show small trends. The RCP 2.6 simulation projects a decrease of sea-ice during the first and an increase of sea-ice during the second half of the 21st century. The RCP 8.5 projection depicts a further decrease during the entire 21st century and a perhaps ice-free Antarctic summer by the end of the century.

Outlook

Overall, the Arctic sea-ice extent is well represented in the MPI-ESM model, while sea-ice extent in the Antarctic is underestimated. The causes for these model deviations have to be investigated in follow-up studies. In another follow-up study, the evaluation will be repeated for decadal model simulations within the MiKlip ClimVal Project. It is an interesting question how the sea-ice distribution will differ in the shorter initialized simulations compared to the free-running simulations that have been analyzed here. Beyond the sea-ice concentration and extent, the sea-ice thickness is an important parameter for sea-ice projections and should be further investigated.

Acknowledgements

This work was performed as part of the BMBF MiKlip Climate Model Validation by confronting globally Essential Climate Variables from models with observations (ClimVal project) and the DLR ESMVal (Earth System Model Validation) project.

First of all I want to thank my supervisor Veronika Eyring for making this work possible. She believed in me and encouraged me, especially during the past weeks.

Big thanks go to Klaus-Dirk Gottschaldt. Whenever I had questions or problems with NCL, he had the right answers and helpful tips.

Many thanks go to Sabrina Wenzel and Mattia Righi for supporting me in several Linux and NCL questions.

I want to thank Mary Haley (NCAR) for her support in developing the polar stereographic functions.

Thanks also go to Georg Heygster and Marcus Huntemann for providing the AMSR-E sea-ice data and for their precious clues about sea-ice.

Finally I want to thank the whole DLR-IPA Department 1 for the enjoyable time.

References

- Bitz, C.M. and Polvani, L.M., 2012. Antarctic climate response to stratospheric ozone depletion in a fine resolution ocean climate model. *Geophysical Research Letters*, 39.
- Ballantyne, A.P., Alden, C.B., Miller, J.B., Tans, P.P. and White J.W.C., 2012, Increase in observed net carbon dioxide uptake by land and oceans during the last 50 years, *Nature* 488, 70-72.
- Barry, R.G., M. C. Serreze, J. A. Maslanik, R. H. Preller, 1993. The Arctic Sea Ice-Climate System: Observations and modeling, *Reviews of Geophysics* Volume 31, Issue 4, pages 397–422, November 1993
- Blanchard-Wrigglesworth, E., Bitz, C.M. and Holland, M.M., 2011. Influence of initial conditions and climate forcing on predicting Arctic sea ice. *Geophysical Research Letters*, 38.
- Cavalieri, D. J., C. I. Parkinson, P. Gloersen, and H. J. Zwally. 1997. Arctic and Antarctic Sea Ice Concentrations from Multichannel Passive-microwave Satellite Data Sets: October 1978 to December 1996, User's Guide. NASA Technical Memorandum 104647. 17 pages.
- Cavalieri, D., C. Parkinson, P. Gloersen, J. Comiso, and H. J. Zwally. 1999. Deriving Long-term Time Series of Sea Ice Cover from Satellite Passive-microwave Multisensor Data Sets. *Journal of Geophysical Research* 104(C7):15,803-15,814.
- Cavalieri, D., Parkinson, C., 2008. Antarctic sea ice variability and trends, 1979–2006
- Comiso, Josefino C., Donald J. Cavalieri, Claire L. Parkinson, Per Gloersen, 1997. Passive microwave algorithms for sea ice concentration: A comparison of two techniques, *Remote Sensing of Environment*, Volume 60, Issue 3, June 1997, Pages 357–384
- Emery, W.J., Fowler, C. and Maslanik, J. (1994). Arctic sea ice concentrations from special sensor microwave imager and advanced very high resolution radiometer satellite data. *Journal of Geophysical Research* 99(C9): doi: 10.1029/94JC01413. issn: 0148-0227.
- Fetterer, F., K. Knowles, W. Meier, and M. Savoie. 2002, updated 2007. *Sea Ice Index*. Boulder, CO: National Snow and Ice Data Center. Digital media.
- Giorgetta, M.A. et al., 2013. Climate change from 1850 to 2100 in MPI-ESM simulations for the Coupled Model Intercomparison Project 5. *JAMES*, submitted.
- Gloersen, P and L. Hardis. 1978. The Scanning Multichannel Microwave Radiometer (SMMR) experiment. *The Nimbus 7 Users' Guide*. C. R. Madrid, editor. National Aeronautics and Space Administration. Goddard Space Flight Center, Maryland.
- Gloersen, P., 1983. Calibration of the Nimbus-7 SMMR: II Polarization mixing corrections, *NASA Tech. Memorandum* 84976.
- Grebmeier, J. M., S. E. Moore, J. E. Overland, K. E. Frey, and R. Gradinger, 2010. Biological response to recent Pacific Arctic sea ice retreats, *Eos Trans. AGU*, 91(18), doi: 10.1029/2010EO180001, 161–168 (2010)

Hansen, J., Sato, M., Ruedy, R., Lo, K., Lea, D. W., Medina-Elizade, M., 2006, Global temperature change

Hartmann, J., Albers, F., Argentini, S., Bochert, A., Bonafe, U., Cohrs, W., Conidi, A., Freese, D., Georgiadis, T., Ippoliti, A., Kaleschke, L., Lüpkes, C., Maixner, U., Mastrandionio, G., Ravegnani, F., Reuter, A., Trivellone, G., and Viola, A., 1999. Arctic Radiation and Turbulence Interaction Study (ARTIST), *Reports on Polar Research*, No. 305, Alfred-Wegener-Institute for Polar and Marine Res., Bremerhaven, Germany.

Hibler, W. D. III, 1979, A dynamic thermodynamic sea ice model. *J. Phys. Oceanogr.*, 9, 815-846

Holland, P.R. and Kwok, R., 2012. Wind-driven trends in Antarctic sea-ice drift. *Nature Geoscience*, 5(12): 872-875.

Ilyina, T., Six, K. D., Segschneider, J., Maier-Reimer, E., Li, H. and Nunez-Riboni, I., 2012 (submitted). The global ocean biogeochemistry model HAMOCC: Model architecture and performance as component of the MPI-Earth System Model in different CMIP5 experimental realizations.

IPCC, 2007. Intergovernmental Panel on Climate Change (IPCC), Climate Change 2007: The Physical Science Basis. Contribution of Working Group I to the Fourth Assessment Report of the Intergovernmental Panel on Climate Change, Cambridge, United Kingdom and New York, NY, USA.

Jungclaus, J. H., Keenlyside, N., Botzet, M., Haak, H., Luo, J.-J., Latif, M., Marotzke, J., Mikolajewicz, U., and Roeckner, E., 2006. Ocean circulation and tropical variability in the coupled model ECHAM5/MPI-OM. *Journal of Climate*, Vol. 19, 3952-3972.

Jungclaus, J. H., Fischer, N., Haak, H., Lohmann, K., Marotzke, J., Matei, D., Mikolajewicz, U., Notz, D. and von Storch, J.-S., 2012 (submitted). Characteristics of the ocean simulations in MPIOM, the ocean component of the MPI Earth System Model.

Kattsov, V.M., Ryabinin, V.E., Overland, J.E., Serreze, M.C., Visbeck, M., Walsh, J.E., Meier, W. and Zhang, X.D., 2010. Arctic sea-ice change: a grand challenge of climate science. *Journal of Glaciology*, 56(200): 1115-1121.

Lingenhöhl, D., 2012. Das antarktische Paradoxon, Spektrum

Meier, W., 2012. Record Low Arctic Sea Ice Extent in 2012: An exclamation point on a long term declining trend, NSIDC

Meier, W., 2012. Climate Algorithm Theoretical Basis Document (C-ATBD) Passive Microwave Sea Ice Concentration, Climate Data Record (CDR) Program, www.
http://nsidc.org/data/docs/noaa/g02202_ice_conc_cdr/pdf/Sealce_CDR_CATBD_final.pdf

Meinshausen, M., Smith, S.J., Calvin, K., Daniel, J.S., Kainuma, M.L.T., Lamarque, J.F., Matsumoto, K., Montzka, S.A., Raper, S.C.B., Riahi, K., Thomson, A., Velders, G.J.M. and van Vuuren, D.P.P., 2011. The RCP greenhouse gas concentrations and their extensions from 1765 to 2300. *Climatic Change*, 109(1-2): 213-241.

Moss, R.H., Edmonds, J.A., Hibbard, K.A., Manning, M.R., Rose, S.K., van Vuuren, D.P., Carter, T.R., Emori, S., Kainuma, M., Kram, T., Meehl, G.A., Mitchell, J.F.B., Nakicenovic, N., Riahi, K., Smith, S.J., Stouffer, R.J., Thomson, A.M., Weyant, J.P. and Wilbanks, T.J., 2010. The next generation of scenarios for climate change research and assessment. *Nature*, 463(7282): 747-756.

Murray, R. J., and Simmonds, I., 1995. Responses of climate and cyclones to reductions in Arctic winter sea ice, *J. Geophys. Res.*, 100, 4791– 4806, doi:10.1029/94JC02206.

Notz, D., F. A. Haumann, H. Haak, J. H. Jungclaus and J. Marotzke, 2013. Arctic sea-ice evolution as modeled by MPI-ESM, doi: 10.1002/jame.20016, JAMES, accepted.

Perovich, D. K., Polashenski, C., 2012. Albedo evolution of seasonal Arctic sea ice, *GEOPHYSICAL RESEARCH LETTERS*, VOL. 39, L08501, doi: 10.1029/2012GL051432, 2012

Rayner, N.A., Parker, D.E., Horton, E.B., Folland, C.K., Alexander, L.V., Rowell, D.P., Kent, E.C. and Kaplan, A., 2003. Global analyses of sea surface temperature, sea ice, and night marine air temperature since the late nineteenth century, *J. Geophys. Res.*, 108(D14): 4407

Reick, C., Raddatz, T., Brovkin, V. and Gayler, V., 2012 (submitted). The representation of natural and anthropogenic land cover change in MPI-ESM.

Riahi K, Krey V, Rao S, Chirkov V, Fischer G, Kolp P, Kindermann G, Nakicenovic N and Rafai P, 2011. RCP-8.5: Exploring the consequence of high emission trajectories. doi: 10.1007/s10584-011-0149-y

Sigmond, M. and Fyfe, J.C., 2010. Has the ozone hole contributed to increased Antarctic sea ice extent? *Geophysical Research Letters*, 37.

Smith, K.L., Polvani, L.M. and Marsh, D.R., 2012. Mitigation of 21st century Antarctic sea ice loss by stratospheric ozone recovery. *Geophysical Research Letters*, 39.

Spencer, R. W., 2001. The Role of Passive Microwave Radiometers in Climate Monitoring

Spreen, G., Kaleschke, L. and Heygster, G., 2008. Sea ice remote sensing using AMSR-E 89-GHz channels. *Journal of Geophysical Research-Oceans*, 113(C2).

Stevens, B., Giorgetta, M. A., Esch, M., Mauritsen, T., Crueger, T., Rast, S., Salzmann, M., Schmidt, H., Bader, J., Block, K., Brokopf, R., Fast, I., Kinne, S., Kornblueh, L., Lohmann, U., Pincus, R., Reichler, T. and Roeckner, E, 2012. (submitted). The atmospheric component of the MPI-M Earth System Model: ECHAM6

Stroeve, J., Holland, M.M., Meier, W., Scambos, T. and Serreze, M., 2007. Arctic sea ice decline: Faster than forecast. *Geophys. Res. Lett.*, 34(9): L09501.

Stroeve, J.C., Kattsov, V., Barrett, A., Serreze, M., Pavlova, T., Holland, M. and Meier, W.N., 2012. Trends in Arctic sea ice extent from CMIP5, CMIP3 and observations. *Geophysical Research Letters*, 39.

Taylor, K.E., Stouffer, R.J. and Meehl, G.A., 2012. An Overview of Cmip5 and the Experiment Design. *Bulletin of the American Meteorological Society*, 93(4): 485-498.

Thomson AM, Calvin KV, Smith SJ, Kyle GP, Volke A, Patel P, Delgado-Arias S, Bond-Lamberty B, Wise MA, Clarke LE and Edmonds JA, 2011. RCP4.5: A pathway for stabilization of radiative forcing by 2100. doi: 10.1007/s10584-011-0151-4

Turner, J., Comiso, J.C., Marshall, G.J., Lachlan-Cope, T.A., Bracegirdle, T., Maksym, T., Meredith, M.P., Wang, Z.M. and Orr, A., 2009. Non-annular atmospheric circulation change induced by stratospheric ozone depletion and its role in the recent increase of Antarctic sea ice extent. *Geophysical Research Letters*, 36.

van Vuuren DP, Stehfest E, Den Elzen MGJ, Deetman S, Hof A, Isaac M, Klein Goldewijk K, Kram T, Mendoza Beltran A, Oostenrijk R, Van Vliet J and Van Ruijven B, 2011. RCP2.6: Exploring the possibility to keep global mean temperature change below 2 degree C. doi: 10.1007/s10584-011-0152-3

Wang, J and Chameides, B, 2005. Global Warming's Increasingly Visible Impacts, Environmental Defense

Declaration of Authorship

I do solemnly declare that I have written the presented thesis by myself without undue help from a second person others and without using such tools other than that specified. Where I have used thoughts from external sources, directly or indirectly published or unpublished, this is always clearly attributed. Furthermore, I certify that this research thesis or any part of it has not been previously submitted for a degree or any other qualification at the Ludwig-Maximilians-Universität of Munich or any other institution in Germany or abroad.

Date

Signature